Applied Thermal Engineering 184 (2021) 116413

Contents lists available at ScienceDirect

Applied Thermal Engineering

journal homepage: www.elsevier.com/locate/apthermeng

Study of oscillating flows through a novel constructal bifurcation Stirling regenerator

Minjie Yu [a], Feng Xin [b], Xiaotian Lai [a], Hui Xiao [a], Zhichun Liu [a], Wei Liu [a,*]

[a] School of Energy and Power Engineering, Huazhong University of Science and Technology, Wuhan 430074, China
[b] School of Energy and Power Engineering, Changsha University of Science and Technology, Changsha 410114, China

ARTICLE INFO

Keywords:
Constructal bifurcation
Stirling engine
Regenerator
Oscillating flow
Flow resistance

ABSTRACT

High flow resistance in conventional porous regenerators has been an important factor for limiting the overall performance of Stirling engines. Herein, a novel constructal bifurcation regenerator based on constructal concept was developed to reduce the flow resistance in the Stirling regenerator. First, the pressure drop and transient conjugate heat transfer characteristics of oscillating flows through the constructal bifurcation regenerator with various geometrical parameters were investigated by the CFD approach. The results showed that the fluid flow and heat transfer between the acceleration and deceleration phases, as well as the discharge and suction phases, were varied significantly. These differences should be resulted from the local acceleration effect, the formation of eddies in the acceleration phase, and different windward surfaces generated by the regenerator matrix to the fluid in the discharge and suction phases. Additionally, the flow characteristics between the oscillating and steady flows were compared and the local acceleration effect was proven to be the main cause of the difference between them. Then the three-parameters correlation equations of friction factor and Nusselt number for each structure and four master correlation equations with geometrical parameter dependence were built to predict the regenerator performance. Thereafter, the constructal bifurcation regenerators were converted to equivalent porous media, and thus the main porous parameters were obtained for the full Stirling engine simulation in the next studies. Finally, the friction factor and Nusselt number of the constructal bifurcation regenerator were compared with those of other commonly used regenerators. It showed that the constructal bifurcation regenerator had a low flow resistance and moderate heat transfer, thus obtaining a high comprehensive performance. The superior comprehensive performance of the regenerator makes it possible to improve the performance of Stirling engines.

1. Introduction

With the increasingly serious energy and environmental problems, the development of renewable energy utilization technologies becomes imperative [1,2]. Among various technical solutions, Stirling engines have attracted widespread attention. Stirling engines have wide energy adaptability as external combustion engines, which can utilize various renewable energy sources such as solar energy, biomass energy, and industrial waste heat. Additionally, Stirling engines also have a series of advantages including high theoretical efficiency, low noise, low emission, and simple structures [3,4]. However, the specific power and overall efficiency of the Stirling engines are relatively lower than those of internal combustion engines due to the numerous irreversible losses in the actual operation [5]. This has limited the further development and application of the Stirling engines. Therefore, the design of Stirling engines with high efficiency is of great value for facilitating the application of Stirling engines, and thus promoting the utilization of renewable energy and addressing energy and environmental problems.

The regenerator is a crucial component for the Stirling engine to run efficiently. It acts like a thermal sponge that absorbs and releases heat alternatively inside the Stirling engine. The regenerator is placed between the heater and the cooler. When the hot fluid flows from the heater to the cooler, the regenerator absorbs heat from the fluid and then releases heat back to the fluid as the cold fluid flows from the cooler to the heater. Therefore, the heat absorbed through the heater from the reservoir decreases significantly, and the engine thermal efficiency is improved. Generally, the heat released to the fluid in the regenerator can reach four times the heat absorbed through the heater during a cycle [6]. At present, the conventional porous media such as woven screens and

* Corresponding author.
E-mail address: w_liu@hust.edu.cn (W. Liu).

https://doi.org/10.1016/j.applthermaleng.2020.116413
Received 8 August 2020; Received in revised form 29 October 2020; Accepted 29 November 2020
Available online 3 December 2020
1359-4311/© 2020 Elsevier Ltd. All rights reserved.

Nomenclature

A	dimensionless inclined angle
a, b, c, a_2, b_2, c_2	correlation equation coefficients
C_2	inertial resistance coefficient, m^{-1}
$c_{p,f}$	specific heat at constant pressure of the fluid, J/(kg·K)
$c_{p,s}$	specific heat at constant pressure of the matrix solid, J/(kg·K)
D	regenerator diameter, m
d_c	central circular rod diameter, m
d_h	hydraulic diameter, m
d_w	wire diameter, m
f_{ast}	friction factor in the actual steady flow
f_{os}	oscillating flow friction factor
f_{st}	steady flow friction factor
h	total heat transfer coefficient between the surface of the matrix solid and the fluid per unit length, W/(m^3·K)
h_c	convective heat transfer coefficient between the surface of the matrix solid and the fluid, W/(m^2·K)
K	permeability, m^2
k	turbulent kinetic energy, m/s^2
L	regenerator length, m
Nu	Nusselt number
p	pressure, Pa
p_0	average pressure of a cycle, Pa
p_{ast}	pressure in the actual steady flow, Pa
p_{max}	amplitude of pressure variation in the oscillating flow, Pa
p_{out}	pressure at the outlet of the regenerator, Pa
q	heat flux of the matrix solid to the fluid, W/m^2
Re_h	Reynolds number
s	wire mesh pitch, m
S	dimensionless wire mesh pitch
S_f	resistance source term, Pa/m
S_{mx}	regenerator matrix surface area, m^2
t	time, s
T_f	temperature of the fluid, K
$T_{f,i}$	mean fluid temperature at the interface between the fluid and solid, K
T_s	temperature of the matrix solid, K
$\boldsymbol{u}$	velocity vector, m/s
u	velocity, m/s
u_{in}	velocity at the inlet of the regenerator, m/s
u_{max}	amplitude of inlet velocity in the oscillating flow, m/s
V	total volume of the regenerator, m^3
V_{mx}	regenerator matrix volume, m^3
x, y, z	coordinate axis

Greek symbols

α	inclined angle, °
α_r	specific surface area of the regenerator, m^{-1}
γ	porosity
ε	turbulent dissipation rate, m^2/s^3
θ	crank angle, °
λ_{ci}	swirling strength, s^{-1}
λ_f	thermal conductivity of the fluid, W/(m·K)
λ_s	thermal conductivity of the matrix solid, W/(m·K)
μ	viscosity, Pa·s
ρ	density, Kg/m^3
ρ_f	density of the fluid, Kg/m^3
ρ_s	density of the matrix solid, Kg/m^3
ω	engine angular frequency, rad/s

metal foam are most commonly used as the regenerator matrix, which are called conventional regenerators in this paper. These regenerators show great superiority in heat transfer between the fluid and the solid due to the large surface area of the matrix. However, the drawback of the conventional regenerator is the high flow resistance, which takes up most of the total flow resistance inside the Stirling engine [7]. The high flow resistance will lead to a large pressure loss for the fluid, and hence decrease the power output and efficiency of the Stirling engine. Accordingly, the optimization design of the regenerator with low flow resistance is of vital importance to the improvement of the Stirling engine performance.

There have been a number of researches of the Stirling regenerators in the public literature, most of which are about the conventional regenerators. Analytical studies were developed to discuss the effects of the temperature oscillation [8,9] and temperature difference [10] in the regenerators on the Stirling engine's performance. Experiments were conducted to build the correlations of friction factor [11] and Nusselt number [12] for the woven screen and metal felt matrixes under the oscillating flow. Other experimental studies detected the energy dissipation caused by the asymmetry of the temperature in the regenerator [13] and involved the optimization of the matrix material and porosity for the stationary regenerator [14] and the moving regenerator [15]. A combined analytical and experimental study revealed how the number of sub-regenerators and the regenerator thermal mass ratio influenced the regenerative effectiveness of the Stirling engine [16]. Numerical simulations were developed to investigate the pressure drop [17] and heat transfer [18] characteristics in the woven wire regenerator matrix, and model the woven screen regenerator as porous media [19]. Other numerical studies discussed the parameter influence of the stationary regenerator [20] and moving regenerator [21] on the power output and thermal efficiency of the Stirling engine. Combined numerical and experimental investigations characterized the fluid flow [22] and thermal [23] phenomenon of oscillating flows through the different wire mesh regenerators. These studies have played a crucial role in understanding the fluid flow and heat transfer mechanisms in the conventional regenerators and expounding the effects of them on the Stirling engine performance, but little attention was paid to solving the problem of the high flow resistance in the conventional regenerators.

In order to avoid the high flow resistance using conventional Stirling regenerators, researchers have tried to design new regenerators with low flow friction. Parallel geometry type regenerators have been one of the most promising regenerators due to their small friction factor [24]. A novel parallel wire regenerator with the matrix wire parallel to the flow was developed by Nam et al. [25]. The flow friction factor of this type of regenerator was found to be three to five times smaller than that of the screen regenerator. A micro-channel type porous-sheets regenerator as a substitution of the conventional screen regenerator for reducing flow friction loss was designed by Li et al. [26]. Lower total loss of effective power and higher thermal effectiveness were obtained for the porous-sheets regenerator compared with the conventional regenerator. Additionally, a new circular-shaped miniature-channels regenerator was presented and investigated by Alfarawi et al. [6,27]. The results showed that higher cooling power was generated by the engine with the new miniature-channels regenerator compared to the engine with the random fiber regenerator. Recently, a new robust foil regenerator [28] was tested to investigate the fluid flow and heat transfer characteristics under oscillating flow. The robust foil regenerator was proved to have better performance than the woven screen regenerator. Besides the parallel geometry type regenerator, other regenerators such as the segmented-involute-foil regenerator [29], the layered-plate type regenerator [30], the regenerators based on lattice structures [31], and regenerators fabricated with an array of pillars [32] were developed to

obtain the low pressure drop in the regenerators.

Theoretically, a regenerator with the heat transfer surface parallel to the flow has the lowest flow resistance but accompanied by relatively poor heat transfer performance. Conversely, a regenerator with the heat transfer surface perpendicular to the flow has the best heat transfer performance and high flow resistance [15]. Therefore, in this study, a novel constructal bifurcation regenerator with the heat transfer surface inclined to the flow direction was developed to reduce flow resistance and meanwhile avoid the poor heat transfer performance. To obtain a large specific surface area and realize the relatively even distribution of the fluid inside the regenerator, the structure of the regenerator matrix was designed based on constructal concept. Over the past two decades, the constructal method has been applied extensively in the structure design and optimization [33] of various engineering processes [34–37]. According to extensive constructal research and practice, the bifurcation type structure [38–40] commonly used in constructal design has repeatedly been proven as an effective design method for achieving superior performance. Therefore, in this work, the bifurcation type structure was employed to design the regenerator matrix. Considering that the fluid in the regenerator is under oscillating flow condition, a numerical study of oscillating flows through the constructal bifurcation regenerator was conducted to analyze the pressure drop and heat transfer characteristics. A woven screen regenerator matrix with a similar structure was investigated under the same conditions to validate the numerical simulation. Moreover, the effects of different geometrical parameters on the fluid flow and thermal performance were investigated. Then the three-parameter correlation equations of friction factor and Nusselt number for regenerators with different geometrical parameters were developed, and four master correlation equations were summarized by introducing geometrical parameters. After that, the constructal bifurcation regenerators were converted to equivalent porous media and thus the main porous parameters were obtained for the future Stirling engine simulations. Finally, friction factor and Nusselt number comparisons between the constructal bifurcation regenerator and other usually used regenerators were conducted.

2. Regenerator model

2.1. Regenerator geometry description

The scheme of the constructal bifurcation regenerator is displayed in Fig. 1. The regenerator is cylindrical with the diameter D and length L being 20 mm and 100 mm, respectively. The regenerator matrix is made of numerous layers of wire mesh attached to the central circular rod, and each layer of wire mesh consists of six bifurcation-shaped structure units. The wire mesh layer is separated from each other at the same pitch to generate a relatively even flow space and diminish the axial heat conduction loss. Additionally, the inclined angle between the wire mesh and central rod is less than 90° to eliminate most flow stagnation points, hence the flow resistance is effectively reduced. The wire diameter d_w is constant with equaling 1 mm. The central circular rod diameter d_c is set as 2 mm. Various wire mesh pitches s, 1.5, 2, 2.5, and 3 (mm) and various inclined angles α, 40, 50, 60, and 70 (°) are selected for the regenerator matrix. The porosity of the regenerator varies with the pitch and inclined angle.

Similar to the traditional woven screen regenerator [22], the porosity of the constructal bifurcation regenerator is defined as:

$$\gamma = 1 - \frac{V_{mx}}{V} \tag{1}$$

where V_{mx} and V are the regenerator matrix volume and total volume, respectively.

The hydraulic diameter is defined as [32]:

$$d_h = \frac{4\gamma V}{S_{mx}} = \frac{4\gamma V_{mx}}{S_{mx}(1-\gamma)} \approx \frac{4\gamma}{1-\gamma}\cdot\frac{d_w}{4} = \frac{d_w\gamma}{1-\gamma} \tag{2}$$

where S_{mx} is the regenerator matrix surface area.

The specific surface area of the regenerator is calculated as [20]:

$$\alpha_r = \frac{S_{mx}}{V} = \frac{(1-\gamma)S_{mx}}{V_{mx}} \approx \frac{4(1-\gamma)}{d_w} \tag{3}$$

The major geometrical parameters of the constructal bifurcation regenerators studied in this paper are summarized and compared in Table 1.

2.2. Governing equations

The governing equations describing the mass, momentum and energy conservations in the constructal bifurcation regenerator are developed based on the following assumptions:

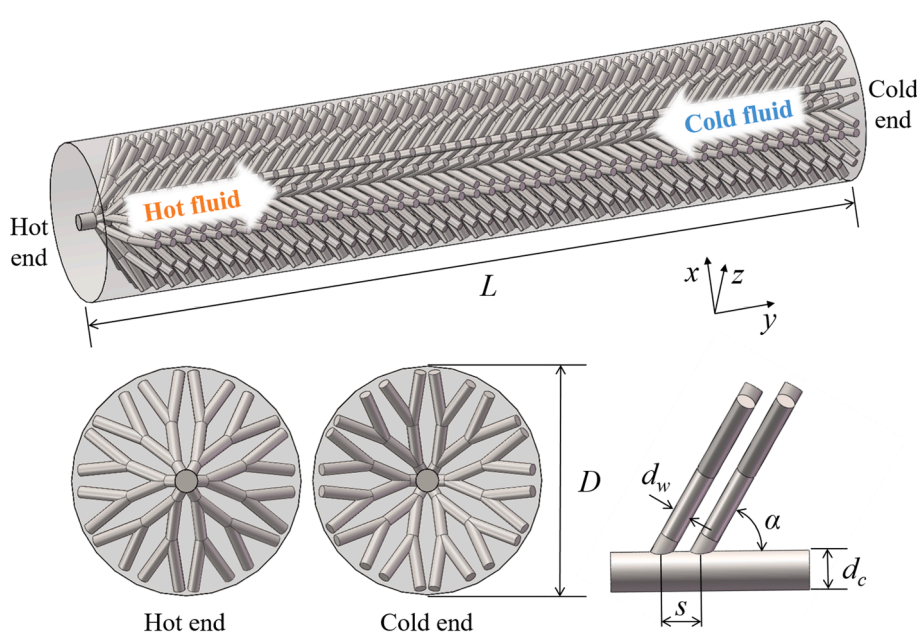

Fig. 1. Scheme of the constructal bifurcation regenerator.

Table 1
Geometrical parameters of the constructal bifurcation regenerators studied in this paper.

Number	Regenerator and wire mesh dimensions (mm)	Pitch (mm)	Inclined angle (°)	Porosity	Hydraulic diameter(mm)	Specific surface area(1/m)
#1	Regenerator	1.5	60	0.742	2.876	1032
#2	length $L = 100$	2	60	0.802	4.051	792
#3	diameter $D = 20$	2.5	60	0.838	5.173	648
#4	Wire mesh	3	60	0.866	6.463	536
#5	wire diameter $d_w = 1$	2	40	0.780	3.545	880
#6	rod diameter $d_c = 2$	2	50	0.798	3.950	808
#7		2	70	0.815	4.405	740

- The fluid flow is unsteady in the regenerator,
- The fluid (helium) is viscous and incompressible in the regenerator,
- The physical properties of the fluid vary with temperature,
- The radiative heat transfer between the fluid and solid (copper) is neglected,
- The gravity and viscous heating of the fluid is neglected.

Therefore, the governing equations can be written as [18,41]:
The mass conservation equation:

$$\frac{D\rho}{Dt} + \rho\nabla\cdot\boldsymbol{u} = 0 \tag{4}$$

where ρ, t, and $\boldsymbol{u}$ denote the density, time, and velocity vector, respectively.

The momentum conservation equation:

$$\rho\frac{D\boldsymbol{u}}{Dt} = -\nabla p - \frac{2}{3}\nabla[\mu(\nabla\cdot\boldsymbol{u})] + \nabla\cdot[\mu(\nabla\boldsymbol{u} + (\nabla\boldsymbol{u})^T)] \tag{5}$$

where p and μ refer to the pressure and viscosity, respectively. $\nabla\boldsymbol{u}$ and $(\nabla\boldsymbol{u})^T$ represent two tensors.

The first term in the momentum Eq. (5) can be decomposed into local derivative term and convective derivative term, then the momentum conservation equation is written as:

$$\rho\frac{\partial\boldsymbol{u}}{\partial t} + \boldsymbol{u}\cdot\nabla(\rho\boldsymbol{u}) = -\nabla p - \frac{2}{3}\nabla[\mu(\nabla\cdot\boldsymbol{u})] + \nabla\cdot[\mu(\nabla\boldsymbol{u} + (\nabla\boldsymbol{u})^T)] \tag{6}$$

where the first term on the left-hand side denotes the local acceleration force, the second term denotes the convective acceleration force (or called inertial force), the first term on the right-hand side is the surface force, and the last two terms are the viscous force. Hence, the surface force imposed on the control volume is the sum of the local acceleration force, convective acceleration force, and viscous force. In the steady flow, the local acceleration force is equal to 0 (N).

The energy conservation equation for the fluid:

$$\rho_f c_{p,f}\frac{DT_f}{Dt} = \nabla\cdot(\lambda_f\nabla T_f) + \frac{Dp}{Dt} + h(T_s - T_f) \tag{7}$$

The energy conservation equation for the matrix solid:

$$\rho_s c_{p,s}\frac{\partial T_s}{\partial t} = \nabla\cdot(\lambda_s\nabla T_s) + h(T_f - T_s) \tag{8}$$

where T_f, ρ_f, $c_{p,f}$, and λ_f denote the temperature, density, specific heat at constant pressure and thermal conductivity for the fluid, respectively. Additionally, T_s, ρ_s, $c_{p,s}$, and λ_s are the temperature, density, specific heat at constant pressure and thermal conductivity for the matrix solid, respectively. h (W/m^{3}K) is the total heat transfer coefficient between the surface of the matrix solid and the fluid per unit length.

2.3. Flow and heat transfer in the regenerator

The schematic of oscillating flows through the constructal bifurcation regenerator is shown in Fig. 2. For a Stirling engine, hot end (always set to 0 mm in the paper) is connected to the heater, while the cold end (always set to 100 mm in the paper) is connected to the cooler. The fluid flows back and forth periodically between the hot and cold ends of the regenerator due to the reciprocating motion of pistons. In a cycle, the hot fluid first flows from the hot end to the cold end and releases heat to the matrix. This phase is called the discharge phase. Then the cold fluid flows from the cold end back to the hot end and absorbs the heat stored in the matrix, which is called the suction phase. Obviously, in the discharge and suction phases, the regenerator matrix will generate different windward surfaces to the fluid, leading to different pressure drop and heat transfer characteristics. In addition, in both discharge and suction phases, the fluid will undergo acceleration and deceleration processes. The flow and heat transfer in these two processes will be different as well due to the effect of fluid local acceleration and the formation of eddy structures.

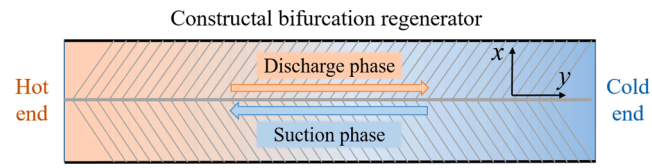

Fig. 2. Schematic of oscillating flows through the constructal bifurcation regenerator.

In most studies of Stirling regenerators, the Reynolds number is defined using hydraulic diameter rather than wire diameter. Hence, the Reynolds number can be calculated as [12]:

$$Re_h = \frac{ud_h\rho_f}{\mu} \tag{9}$$

where u is the velocity of the fluid.

An oscillating flow friction factor is defined as [22]:

$$f_{os} = \frac{\Delta p}{\frac{1}{2}\rho u^2\frac{L}{d_h}} \tag{10}$$

where Δp refers to the pressure drop of the regenerator in the oscillating flow. According to the momentum equation, the pressure drop is composed of local acceleration resistance, convective acceleration resistance, and viscous resistance. Thereby, f_{os} is a dimensionless criterion for representing these three terms of flow resistance. It is worth mentioning that in most other works of oscillating flows in regenerators, the pressure drop at the maximum velocity of a cycle is usually employed to calculate the friction factor in the oscillating flow, at which point the local acceleration is very small and the resistance caused by it can be negligible compared to other resistance. However, in this study, the instantaneous pressure drop characteristics of the regenerator in a cycle are one of our main research focuses. To achieve this end, we have to obtain the pressure drop data at different points in the cycle. Whereas, at most moments of the cycle, especially at a moment of low velocity, the local acceleration resistance accounts for a large part in the total pressure drop. Therefore, it is inappropriate to ignore the local acceleration effect as before.

The regenerator will be converted into the equivalent porous media to be embedded into the full Stirling engine model for studying the effects of the regenerator on the performance of the engine in the next

studies. To obtain the critical porous model parameters, a porous model is developed by the addition of an extra source term to the standard fluid flow equation. The porous model momentum equation can be written as:

$$\rho\frac{\partial(\gamma\boldsymbol{u})}{\partial t}+\boldsymbol{u}\cdot\nabla(\gamma\rho\boldsymbol{u}) = -\gamma\nabla p-\frac{2}{3}\nabla[\gamma\mu(\nabla\cdot\boldsymbol{u})]+\nabla\cdot[\gamma\mu(\nabla\boldsymbol{u}+(\nabla\boldsymbol{u})^T)]+\gamma S_f \tag{11}$$

The source term S_f describes the drag force effect of the regenerator matrix to the fluid, which is composed of two parts of a viscous loss term and an inertial loss term [42]:

$$S_f = -(\frac{\mu}{K}\boldsymbol{u}+\frac{C_2}{2}\rho|u|\boldsymbol{u}) \tag{12}$$

where K and C_2 denote the permeability and inertial resistance coefficient, respectively.

In porous model, the convective acceleration force and viscous force can be ignored, thus the momentum Eq. (11) can be simplified as:

$$\nabla p = -(\frac{\mu}{K}\boldsymbol{u}+\frac{C_2}{2}\rho|u|\boldsymbol{u})-\rho\frac{\partial\boldsymbol{u}}{\partial t} \tag{13}$$

Therefore, the pressure drop of the regenerator is the sum of the viscous loss, inertial loss, and local acceleration loss:

$$\Delta p = (\frac{\mu}{K}u+\frac{C_2}{2}\rho u^2+\rho\frac{\partial u}{\partial t})L \tag{14}$$

According to Eq. (14), the porous parameters permeability K and inertial resistance coefficient C_2 are independent of the local acceleration. Hence, to obtain the K and C_2, the local acceleration resistance has to be subtracted from the total pressure drop in the oscillating flow. Therefore, a steady flow friction coefficient f_{st}, which eliminates the local acceleration effect, is defined to calculate the two porous parameters.

$$f_{st} = \frac{\Delta p-\rho\frac{\partial u}{\partial t}L}{\frac{1}{2}\rho u^2\frac{L}{d_h}} \tag{15}$$

f_{st} is the dimensionless criterion to characterize the viscous resistance and convective acceleration resistance, which represents the structure-dependent inherent resistance characteristics of the constructal bifurcation regenerator. Additionally, since it only eliminates the local acceleration effect when compared with the oscillating flow friction factor, the f_{st} is analogous to the friction factor at the maximum velocity of a cycle in the oscillating flow, which is different from the friction factor in an actual steady flow.

By substituting Eq. (14) into Eq. (15), f_{st} can be written as:

$$f_{st} = \frac{2d_h^2}{KRe_h}+C_2d_h \tag{16}$$

Referring to previous studies of Stirling regenerator [11,17,22], a correlation equation of steady flow friction factor is proposed as following form:

$$f_{st} = \frac{a}{Re_h}+bRe_h^c \tag{17}$$

Combining Eqs. (16) and (17), the permeability and inertial resistance coefficient can be calculated as:

$$K = \frac{2d_h^2}{a} \tag{18}$$

$$C_2 = \frac{bRe_h^c}{d_h} \tag{19}$$

With respect to the convective heat transfer between the fluid and the surface of the regenerator matrix, a convective heat transfer coefficient is defined as:

$$h_c = \frac{q}{T_s-T_f} \tag{20}$$

where q is the heat flux of the matrix solid to the fluid.

The total heat transfer coefficient per unit length and the convective heat transfer coefficient has the relationship as follows [20]:

$$h = \alpha_r h_c \approx \frac{4(1-\gamma)}{d_w}h_c \tag{21}$$

Then the Nusselt number is defined based on the convective heat transfer coefficient as [19]:

$$Nu = \frac{h_c d_h}{\lambda_f} \tag{22}$$

Similar to the friction factor, a correlation equation of the Nusselt number is determined as follows [18]:

$$Nu = a_2+b_2Re_h^{c_2} \tag{23}$$

The above correlation equation will be used to calculate the convective heat transfer coefficient in the porous model of the regenerator in future studies.

2.4. Solution procedure

2.4.1. Boundary conditions and initialization

During the operation of Stirling engines, the fluid flows back and forth periodically between the hot end and the cold end of the regenerator. Accordingly, the velocity, temperature, and pressure of the fluid in the regenerator vary periodically. Since the actual oscillating boundary conditions of the regenerators are complex, sinusoidal velocity and pressure profiles are set as the simplified oscillating boundary conditions [43]. Hence, the regenerator simulation is conducted by using the following boundary conditions:

Inlet (hot end) boundary: sinusoidal velocity profiles

$$u_{in} = u_{max}sin(\theta) = u_{max}sin(\omega\cdot t) \tag{24}$$

Outlet (cold end) boundary: sinusoidal pressure profiles

$$p_{out} = p_0-p_{max}cos(\theta) = p_0-p_{max}cos(\omega\cdot t) \tag{25}$$

where u_{in} denotes the velocity at the inlet of the regenerator, u_{max} denotes the amplitude of inlet velocity in the oscillating flow (21.9 m/s), θ represents the crank angle, and ω is the engine angular frequency (60π rad/s). Additionally, p_{out} denotes the pressure at the outlet of the regenerator, p_0 represents the average pressure of a cycle (1.5 MPa), and p_{max} is the amplitude of pressure variation in the oscillating flow (0.25 MPa). Moreover, the temperature at the hot end and the cold end are set as 800 K and 300 K, respectively. The wall boundary is set as the no-slip wall with the adiabatic condition. Additionally, in this study, the temperature of the regenerator is initialized to a constant value of 800 K (hot end temperature).

2.4.2. Solver settings

The governing equations are solved using the commercial code of ANSYS fluent 16.0. The code uses the finite volume method (FVM) to discretize the differential equations. In the FVM, the computational domain is divided into a series of non-repetitive control volumes, each of which is represented by a node, and the conservation differential equations to be solved are integrated for space and time in any control volume and a time interval. The pressure-based segregated solver is adopted with the PISO scheme of pressure–velocity coupling. The second order upwind discretization scheme of space and second order implicit discretization scheme of time are chosen for the continuity, momentum, and energy equations. In addition, the fluid flow in the regenerator is considered to be turbulent for most of a cycle. Hence, the RNG k-ε turbulent model is selected for its excellent prediction

capability in a highly swirling pattern and separation prevail flow [44]. In this study, the time step is fixed and set to 1/360 of a cycle.

3. Grid independence study and model validation

3.1. Grid independence study

A grid independence study is performed to improve the accuracy of the numerical investigation, as shown in Fig. 3. The effects of three grid systems with different grid number 8240000, 13440000, and 18,580,000 on the pressure drop between the inlet and outlet, the mean fluid temperature at the interface between the fluid and solid ($T_{f,i}$), the friction factor, and the Nusselt number of the constructal bifurcation regenerator are tested. When the grid number increases from 13,440,000 to 18580000, the average differences of the pressure drop, the mean fluid temperature at the interface $T_{f,i}$, the friction factor, and the Nusselt number are 1.2%, 0.07%, 2%, and 2.6%, respectively, and the maximal differences of them are 4.8%, 0.19%, 3.4%, and 4.3%, respectively. Hence, considering both accuracy and calculation time, the grid system with 13,440,000 grid elements is adopted for the calculation.

3.2. Model validation

It is worth mentioning that it is difficult to find previously published experimental works with the same geometrical and operating parameters as the present study for model validation. Additionally, due to the complexity of the constructal bifurcation structures, it is difficult for us to manufacture and test them currently. However, the conventional stacked woven screen regenerator matrix has some similarities in structures with the constructal bifurcation regenerator matrix proposed in the present work. On one hand, both regenerators consist of multiple layers of parallel wire mesh. On the other hand, each layer of wire mesh is composed of small cylindrical metal wire with fixed distribution shapes. These structural similarities lead to some similarities in their interactions with the fluid, such as the flow around cylinders and flow separation phenomenon on a micro level and the interaction of fluid flows between different layers of wire mesh on a macro level. Accordingly, it is reasonable to verify the numerical method presented in this study by the conventional woven screen matrix. Herein, an actual geometric model for a small representative portion of the stacked woven screen regenerator matrix is built. A CFD simulation of the woven screen regenerator matrix is conducted under the same solver setting and boundary conditions. The results obtained from the CFD simulation are compared with those obtained from the experiments of Tanaka et al. [12] and Gedeon and Wood [11] to validate the reliability of the

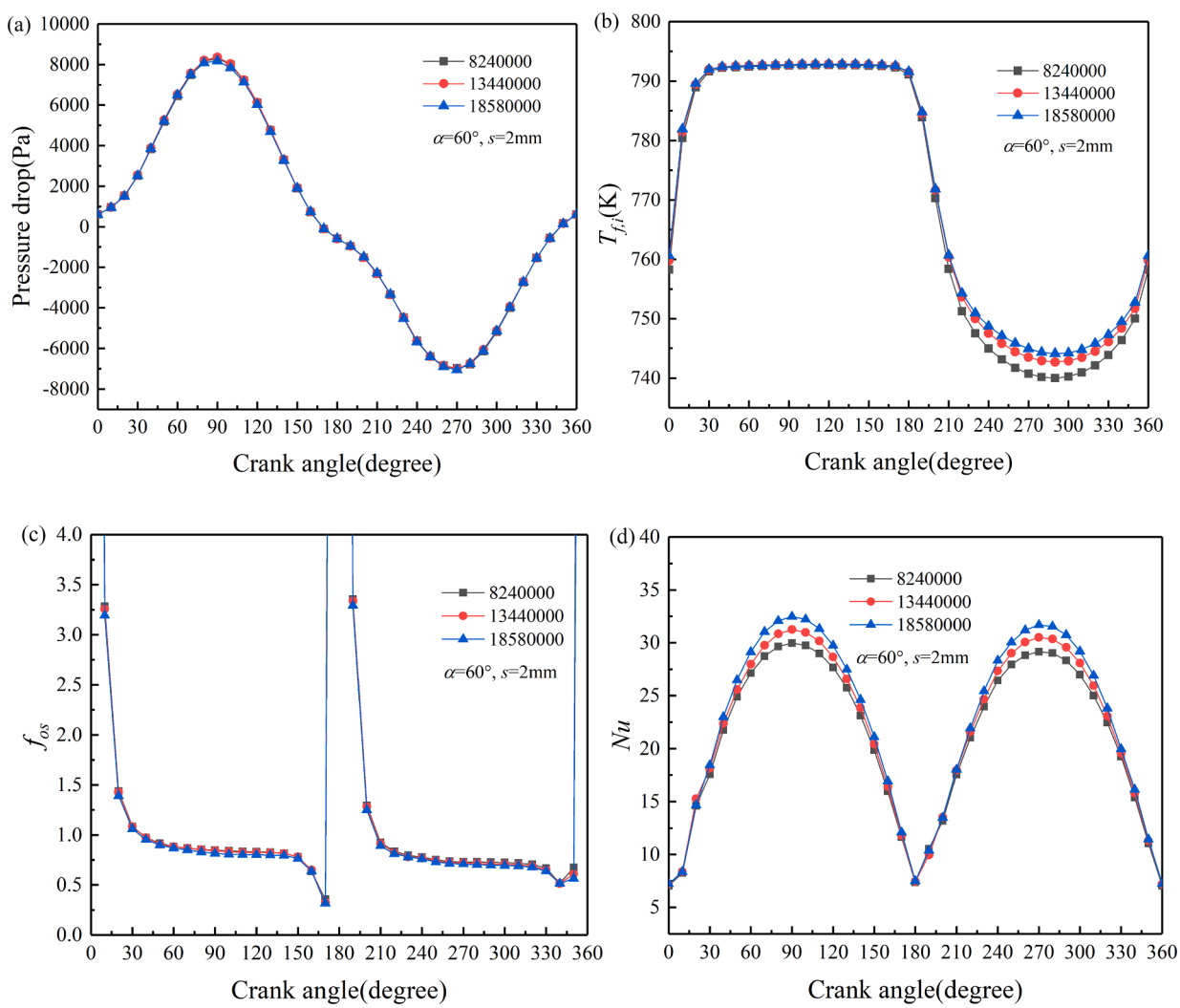

Fig. 3. Grid independence study of the constructal bifurcation regenerator: (a) pressure drop between the inlet and outlet, (b) mean fluid temperature at the interface between the fluid and solid $T_{f,i}$, (c) oscillating flow friction factor, and (d) Nusselt number.

numerical method. The configuration of the stacked woven screen regenerator matrix built in the present study is shown in Fig. 4. The adjacent layers of screens are misaligned, which is more consistent with the configuration of the actual woven screen matrix. The geometrical parameters of the stacked woven screen regenerator matrix are summarized in Table 2. The dimensions of the regenerators tested by Tanaka et al. and Gedeon and Wood are summarized in Table 3. According to Tables 2 and 3, it can be observed that the dimensions of the woven screen regenerator matrix built in the present study are almost in the experimental range of Tanaka et al. and Gedeon and Wood. Therefore, the empirical correlations developed by the experimental works apply to the woven screen regenerator matrix model presented in this paper.

The comparison between the numerical results and experimental results is shown in Fig. 5. Fig. 5(a) illustrates that the friction factor obtained from simulation is in better agreement with the empirical correlation of Gedeon and Wood. The maximum deviation of them is 17.3%. Fig. 5(b) shows that the numerical Nusselt number fits well with the correlation equation proposed by Tanaka et al. with a deviation of less than 17%.

4. Results and discussion

4.1. Pressure drop characteristics

The pressure drop characteristics of oscillating flows through the constructal bifurcation regenerator are analyzed in this section. Fig. 6 presents the fluid flow characteristics in the regenerator. As illustrated in Fig. 6(a) and (c), benefiting from a uniform flow space in the regenerator, the fluid is relatively evenly distributed throughout the regenerator except for a lower velocity in the downstream zone of the bifurcation. This will facilitate the heat transfer between the fluid and the entire regenerator matrix and improve the regenerator effectiveness. Fig. 6(b) shows that there is almost no flow stagnation along the axial direction in the entire flow field of the regenerator, which can efficiently reduce the flow resistance. Additionally, a moderate radial velocity component for the fluid is generated by the inclined wire mesh in the entire flow field, which will intensify the mixing of fluids in different radial zones and increase the temperature difference between the fluid and the regenerator matrix. According to Fig. 6(d), numerous local eddy structures are formatted in the entire regenerator, leading to an enhancement of local convective heat transfer between the fluid and the matrix.

Fig. 7 shows the pressure value of the fluid along the flow direction as the crank angle equals 90°. It is observed that the pressure variation is stepwise and uniform due to the separate and equidistant distribution of wire mesh, but in general, the trend is linear. Fig. 8 shows the variation of pressure drop with length at different crank angles. It can be seen that the pressure drop between the hot end and cold end increases when the crank angle rises from about −10° to 90° and then decreases as the crank angle changes from 90° to about 170°. This is different from the trend that the fluid velocity increases at 0–90° and declines at 90–180°. This phenomenon is mainly caused by the fluid local acceleration effect. At −10 to 0° and 170–180°, the pressure drop caused by a low fluid velocity is not as great as the pressure drop caused by a large local acceleration in the opposite direction, which leads to the opposite direction of the total pressure drop and fluid velocity.

The effects of various wire mesh pitches and inclined angles on the pressure drop through the regenerator are investigated. The pressure drop behaviors in different flow phases of a cycle are presented and compared. Fig. 9 displays the comparison of the pressure gradient in four different phases of a cycle. In both discharge and suction phases, the pressure gradient in the acceleration process is larger than that in the deceleration process. The fluid local acceleration effect is the main cause of this phenomenon. In the acceleration phase, the fluid velocity and local acceleration are in the same direction, and the pressure gradient through the regenerator increases compared with that of the steady flow under the same velocity, while in the deceleration phase, the pressure gradient will be smaller than that of the steady flow at the same velocity due to the opposite direction of the fluid velocity and local acceleration. As the fluid velocity decreases, the local acceleration increases, thus the difference of pressure gradient between the acceleration and

Table 2
Geometrical parameters of the stacked woven screen matrix.

Flow areas (mm^2)	Matrix length (mm)	Wire diameter (mm)	Mesh number	Porosity
1.905 × 1.905	1.54	0.1	100	0.733

Table 3
Dimensions of the stacked woven screen matrix tested by Tanaka et al. and Gedeon and Wood.

	Wire diameter(mm)	Mesh number	Porosity
Tanaka et al.	0.05–0.23	50/100/150/200	0.645–0.754
Gedeon and Wood	0.053–0.094	80/100/200	0.623–0.781

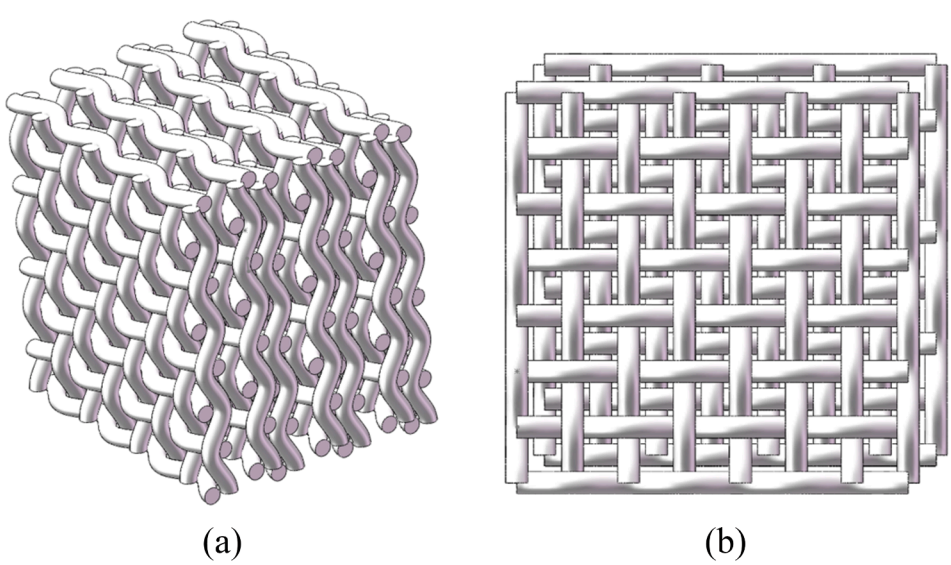

Fig. 4. Configuration of the stacked woven screen matrix: (a) full view and (b) front view.

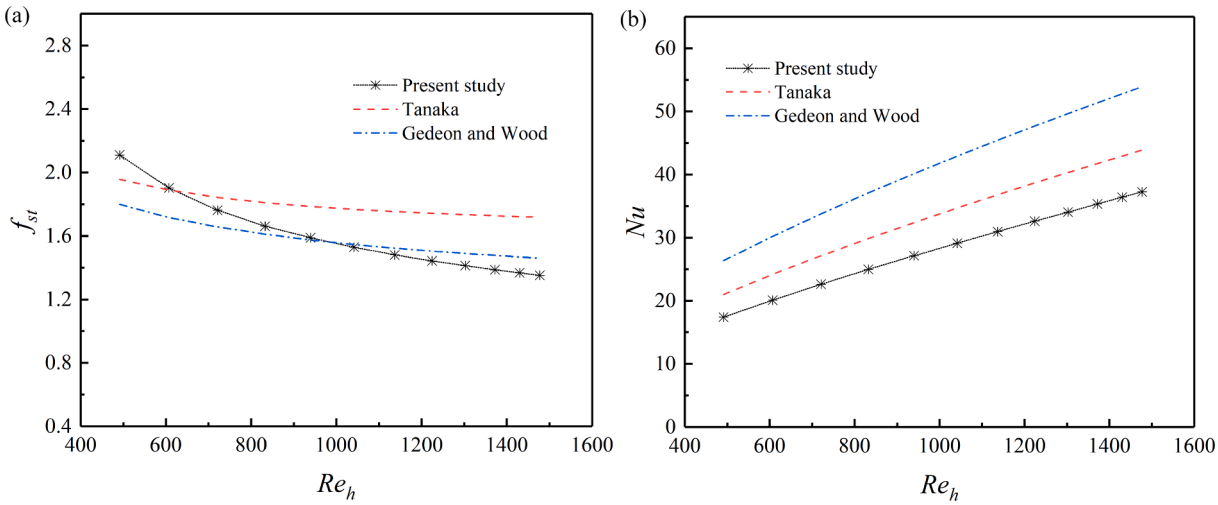

Fig. 5. Comparison between the numerical and experimental results of the stacked woven screen matrix: (a) friction factor and (b) Nusselt number.

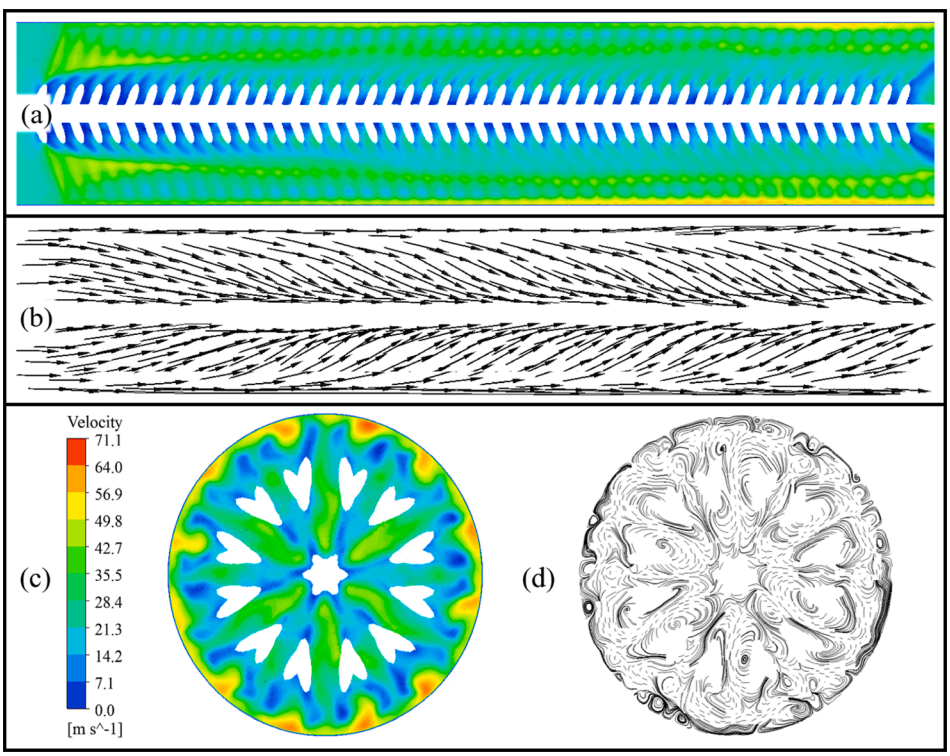

Fig. 6. Fluid flow characteristics of the regenerator at $\theta = 90°$ ($\alpha = 70°$, $s = 2$ mm): (a) velocity profile at the axial section, (b) streamline at the axial section, (c) velocity profile at the middle cross-section, and (d) streamline at the middle cross-section.

deceleration phases increases. Additionally, the pressure gradient in the discharge phase is slightly smaller than that in the suction phase due to different windward surfaces generated by the regenerator matrix. Moreover, the lower average fluid velocity is found in the suction phase due to the higher fluid density in this phase.

Fig. 10 presents the effects of wire mesh pitches on the pressure gradient through the regenerator in different phases of a cycle. It shows that the wire mesh pitch has little effect on the pressure gradient in all phases. Additionally, the average fluid velocity in discharge and suction phases decreases as the wire mesh pitch increases. Fig. 11 illustrates the effect of the inclined angle of wire mesh on the pressure gradient through the regenerator. It is observed that when the inclined angle is less than 60°, the pressure gradient in all phases of the cycle increases with the inclined angle, while after the inclined angle reaches 60°, the inclined angle affects little on the pressure gradient. This is probably because the inclined angle affects the disturbance intensity of the regenerator matrix to the fluid, and thus changes the viscous loss and inertial loss.

Fig. 12 shows the oscillating flow friction factor in different phases of the cycle. As can be seen that for both discharge and suction phases, the friction factor in the acceleration phases is greater than that in the deceleration phase. This phenomenon is consistent with Dellali's work [32] for a regenerator made from an array of pillars and Wang's [45] and Isshiki's [46] works for conventional woven screen regenerators. This is a result of the higher pressure drop in the acceleration phase. The friction factor reaches a limit value at the maximum Reynolds number. This friction factor limit value has been shown to be dependent to the geometrical parameters of the regenerator and the maximum Reynolds

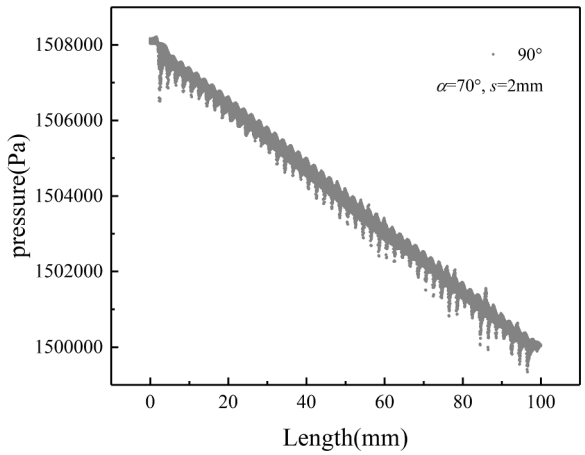

Fig. 7. Pressure value of the fluid with length.

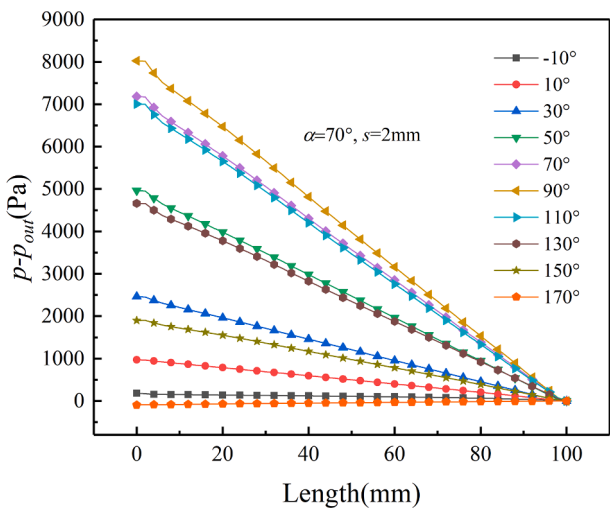

Fig. 8. Pressure drop with length at various crank angles.

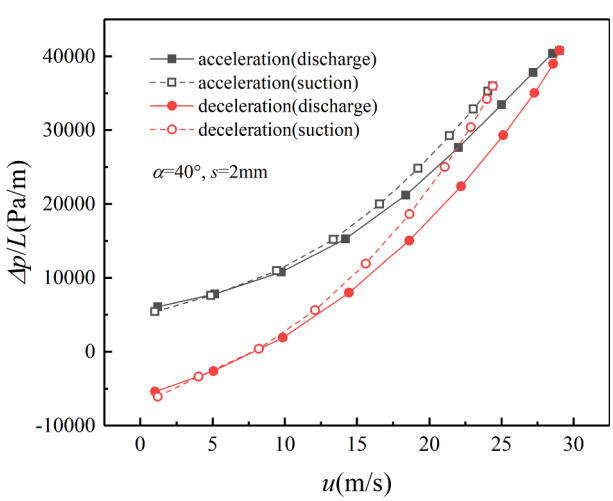

Fig. 9. Pressure gradient in four different phases of a cycle.

number. Furthermore, the maximum Reynolds number is higher in the suction phase, as the density and viscosity of fluid are greater in this phase.

The effects of the wire mesh pitch and the inclined angle on the oscillating flow friction factor are plotted in Figs. 13 and 14, respectively. It is found that the friction factor and the friction factor limit value tend to increase with the increase of the wire mesh pitch (Fig. 13). It indicates that different wire mesh pitches will lead to different flow patterns in the regenerator, though the total pressure drop of the regenerator is nearly the same. Additionally, as the wire mesh pitch raises, the hydraulic diameter of the regenerator matrix will increase, which results in the increase of the maximum Reynolds number. Fig. 14 shows the friction factor and the limit value increase with the inclined angle. This is consistent with the variation of the pressure drop through the regenerator with the inclined angle. Moreover, as the inclined angle increases, the maximum fluid velocity and the hydraulic diameter change little, as a result, the maximum Reynolds number has no significant difference.

The steady flow friction factor defined in this work is calculated and compared with the friction factor in an actual steady flow and the oscillating flow friction factor. Figs. 15 and 16 show the steady flow friction factor under various wire mesh pitches and inclined angles, respectively. The friction factor of the acceleration and deceleration phases appears almost coincident by eliminating the local acceleration effect. This proves that the local acceleration effect is indeed the main cause of the different pressure drop characteristics in these two phases. Moreover, the steady flow friction factor raises significantly with the increase of the wire mesh pitch and the inclined angle. Within the range of geometrical parameters studied in this work, the maximum average friction factor at $\alpha = 60°$, $s = 3.0$ mm is about 3 times of the minimum average friction factor at $\alpha = 40°$, $s = 2.0$ mm. Additionally, 8–26% higher friction factor values are found in the discharge phase than those in the suction phase due to the different windward surfaces of the regenerator matrix to the fluid in these two phases.

As described in Section 2.3, the steady flow friction factor defined in this paper is analogous to the oscillating flow friction factor at the maximum velocity of a cycle and is different from the friction factor in the actual steady flow. Therefore, to explore the relationship between the two friction factor, the friction factor in the actual steady flow (f_{ast}) is calculated through CFD simulation of the actual steady flow and compared with the steady flow friction factor f_{st} defined in the present paper, as illustrated in Fig. 17. The friction factor f_{ast} is defined as:

$$f_{ast} = \frac{\Delta p_{ast}}{\frac{1}{2}\rho u^2 \frac{L}{d_h}} \tag{26}$$

where Δp_{ast} is the pressure drop of the regenerator in the steady flow.

According to Fig. 17, it can be observed that the steady flow friction factor f_{st} is almost consistent with the friction factor in an actual steady flow f_{ast} under two different flow directions, which indicates that the flow resistance characteristics in the steady flow can be represented by the steady flow friction factor f_{st} defined in this study. Additionally, it also proves that the local acceleration effect is the main reason for the difference in pressure drop characteristics between the oscillating and steady flows. That is, if the local acceleration effect is eliminated, for example, when the pressure drop at the maximum velocity of a cycle in the oscillating flow is used to calculate the friction factor, it will be reasonable if the friction factor in the oscillating flow is nearly the same as that in the steady flow.

Fig. 18 presents the comparison of the oscillating flow friction factor and the steady flow friction factor. The oscillating flow friction factor almost declines throughout the whole discharge and suction phases, except for a rapid rise near the 0° and 180° due to the extremely small velocity and large local acceleration. However, for the steady flow friction factor, there are a decrease in the acceleration phase and an increase in the deceleration phase. In terms of the value of the friction factor, in the acceleration phase, the steady flow friction factor is lower than the oscillating flow friction factor, while in the deceleration phase, the steady flow friction factor becomes higher than the latter. The two friction factor tends to be equal at the maximum Reynolds number.

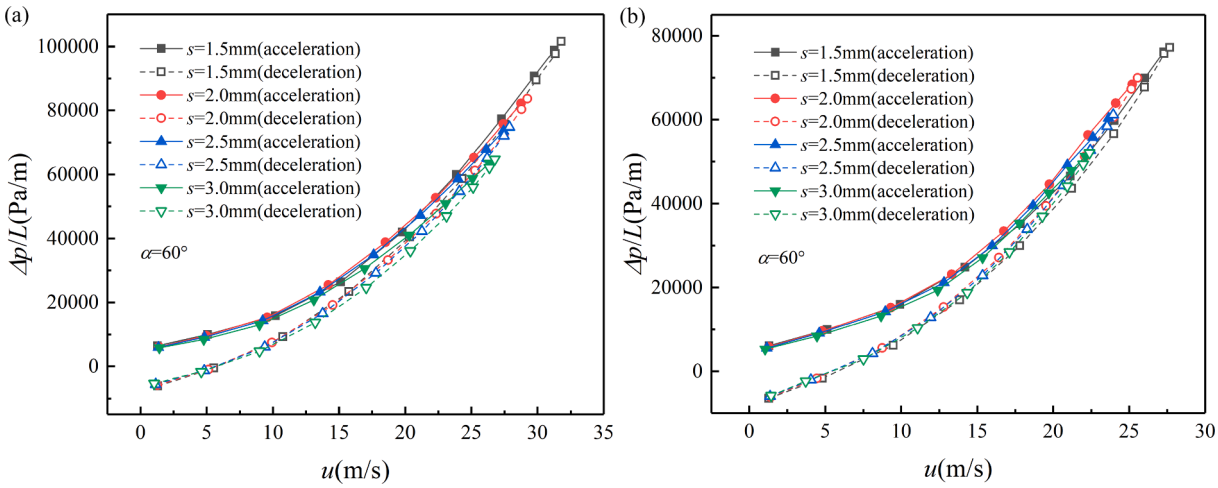

Fig. 10. Pressure gradient through the regenerator under various wire mesh pitches: (a) discharge phase and (b) suction phase.

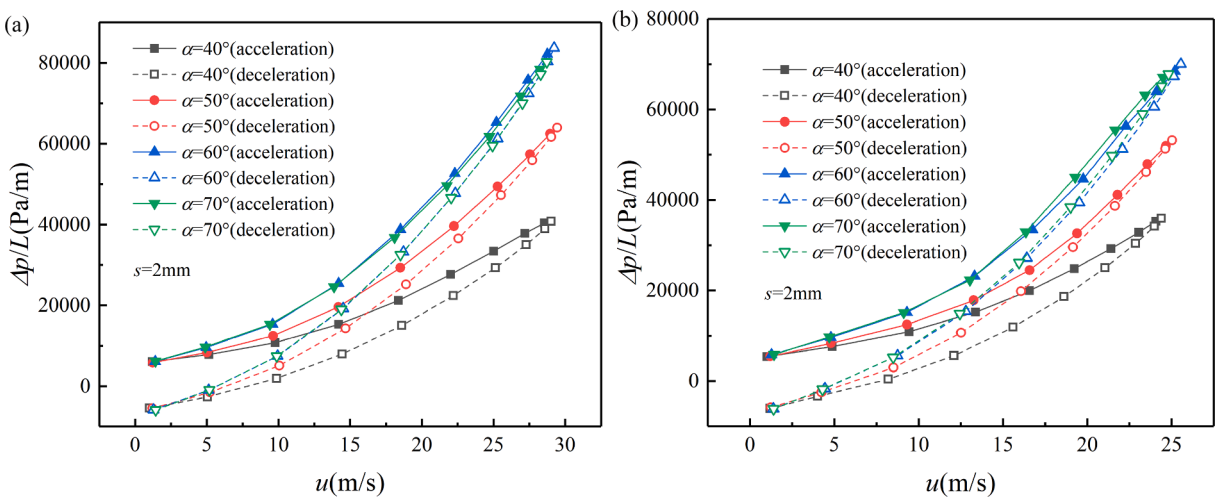

Fig. 11. Pressure gradient through the regenerator under various inclined angles: (a) discharge phase and (b) suction phase.

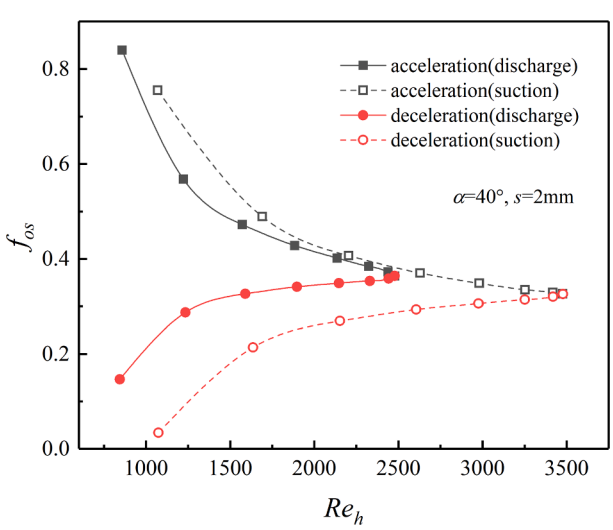

Fig. 12. Oscillating flow friction factor in four different phases of a cycle.

4.2. Heat transfer characteristics

In this section, the heat transfer characteristics of oscillating flows through the constructal bifurcation regenerator are presented. Fig. 19(a) and (b) display the distributions of the local Nusselt number along the flow direction for the regenerators with different geometrical parameters as the crank angle equals 90° and 270°, respectively. The results enable us to understand the inherent mechanism of the difference in heat transfer characteristics between the discharge and suction phases. For the crank angle of 90°, the hot fluid flows in from the hot end of the regenerator and releases heat to the regenerator matrix. As the fluid flows in, the flow begins to be disturbed by the regenerator matrix, which leads to the formation and growth of the eddy in the flow, and thus the convective heat transfer between the fluid and the regenerator matrix is gradually enhanced. After the fluid flows through a part of the regenerator matrix, the flow is nearly fully developed, and the number of eddies reaches the maximum and stops growing, as a result, the heat transfer performance almost keeps constant. As for the crank angle of 270°, the cold fluid flows from the cold end to the hot end and absorbs heat from the regenerator matrix. When the fluid flows in from the cold end, the convective heat transfer rate raises as the flow distance increases due to the increase of the number of eddies. At a distance of about 50 mm from the cold end, the flow is nearly fully developed and the heat transfer performance approaches the maximum. It takes a

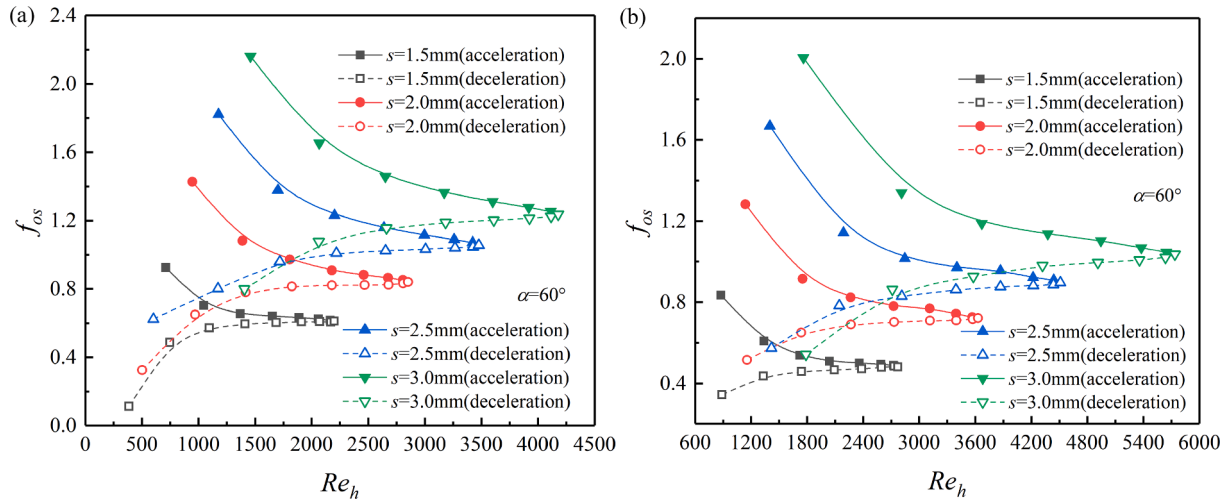

Fig. 13. Oscillating flow friction factor under various wire mesh pitches: (a) discharge phase and (b) suction phase.

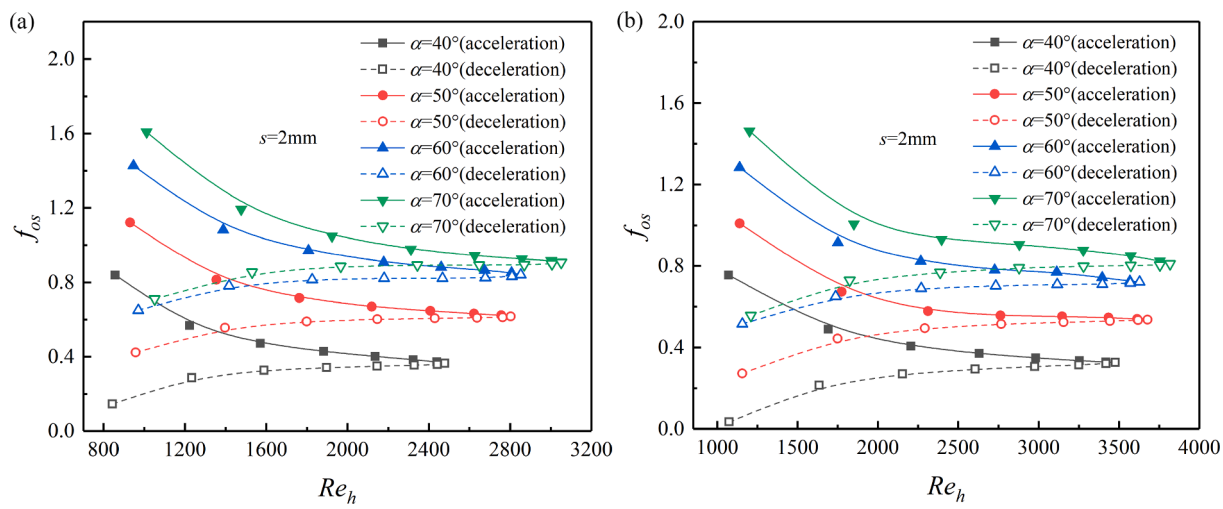

Fig. 14. Oscillating flow friction factor under various inclined angles: (a) discharge phase and (b) suction phase.

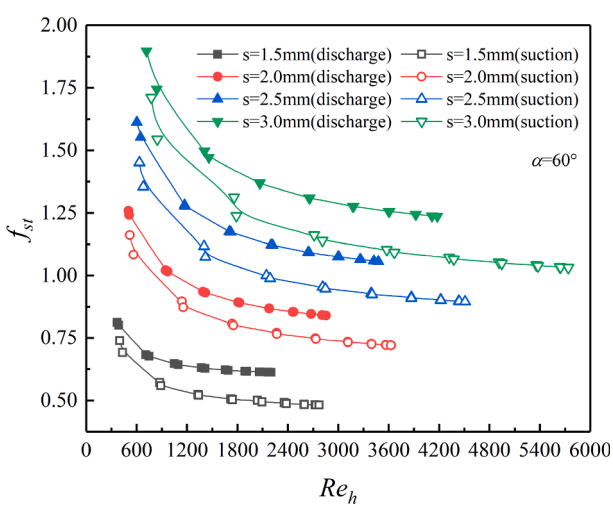

Fig. 15. Steady flow friction factor under various wire mesh pitches.

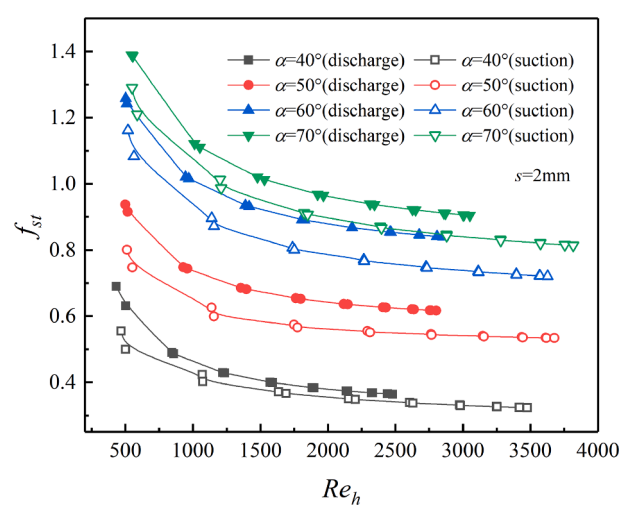

Fig. 16. Steady flow friction factor under various inclined angles.

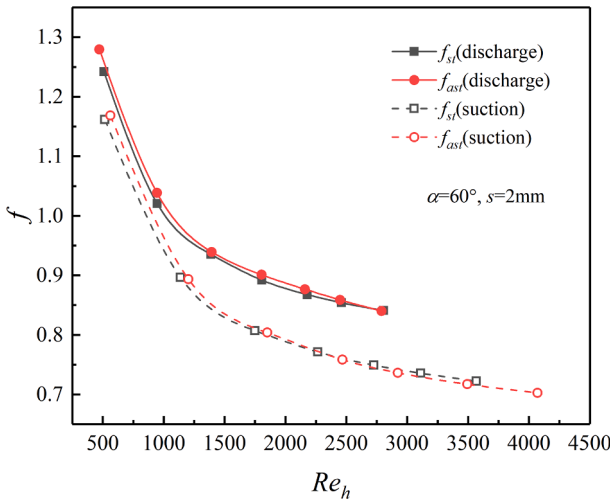

Fig. 17. Comparison of the steady flow friction factor defined in this study and the friction factor in an actual steady flow.

longer flow distance to obtain a fully developed flow at the crank angle of 270° compared with the crank angle of 90°. This is because the regenerator matrix has different windward surfaces to the fluid as the flow is in opposite directions at the two moments. Therefore, the disturbance intensity of the matrix to the flow is different at these two moments, leading to the difference in the formation speed of eddies. Additionally, when the fluid is closed to the hot end, the ability of the matrix to disturb the flow is weakened and the convective heat transfer performance is declined due to the relatively lower local filling rate of the matrix here.

Fig. 20 shows the comparison of Nusselt number under different phases of the cycle. In both discharge and suction phases, the Nusselt number in the acceleration process is lower than that in the deceleration process. This is due to the effect of the formation of eddies in the acceleration phase, as illustrated in Figs. 21 and 22. Fig. 21 shows the variation of the velocity vector at the middle cross-section of the regenerator under different crank angles (the visible eddies are highlighted in red boxes). Fig. 22 displays the average swirling strength λ_{ci} at the middle cross-section in the discharge phase. The swirling strength λ_{ci} was first proposed by Zhou et al. [47] and has been proven to be an effective criterion to represent the strength of the local eddy motion [48].

According to Figs. 21 and 22, in the acceleration phase, the number and strength of eddies raise as the fluid Reynolds number increases, and their peaks appear at the maximum Reynolds number. However, when the fluid velocity begins to decrease in the deceleration phase, the strength of the eddies decreases while the number of them seems to have no significant change, which will lead to a higher number of eddies in the deceleration phase compared to that in the acceleration phase. Moreover, as shown in Fig. 22, the strength of the local eddy motion in the deceleration phase is higher slightly than that in the acceleration phase as well. As a result, both the number and strength of the eddies in the acceleration phase are lower than that in the deceleration phase under the same Reynolds number, resulting in a lower Nusselt number in the former. Additionally, it is also observed in Fig. 20 that the Nusselt number of the discharge phase is higher compared with that of the suction phase under the same Reynolds number due to the different windward surfaces of the regenerator matrix to the fluid under different flow directions. In this study, the regenerator exhibits a 4–40% higher heat transfer performance in the discharge phase than the suction phase.

Figs. 23 and 24 present the effects of the wire mesh pitch and the inclined angle on the Nusselt number, respectively. The interaction between the later layer of wire mesh and the fluid will be weakened by influence of the former layer in the regenerator. As the wire mesh pitch raises, the influence of the former layer of wire mesh decreases, leading to the enhancement of the interaction between the matrix and fluid, thus increasing the heat transfer performance (Fig. 23). Fig. 24 shows that the Nusselt number of the regenerator raises with the increase of the inclined angle. This should be because that the increase of the inclined angle will improve the disturbance intensity of the matrix to the fluid, and then increases the number and intensity of eddies in the flow, which leads to the enhancement of the heat transfer performance.

4.3. Correlation equations for friction factor and Nusselt number

The three-parameters correlation equations for steady flow friction factor and Nusselt number are obtained based on the form of Eqs. (17) and (23). The least square method is employed to calculate the equation coefficients. To eliminate the influence of different flow patterns in the acceleration and deceleration phases, the Nusselt number of the two phases is averaged. Additionally, to distinguish the different effects of the regenerator matrix on the thermo-hydraulic performance in the discharge and suction phases, the correlation equations of these two phases are determined respectively. The correlation equations and critical porous model parameters of the regenerators with different structures in different phases are summarized in Table 4.

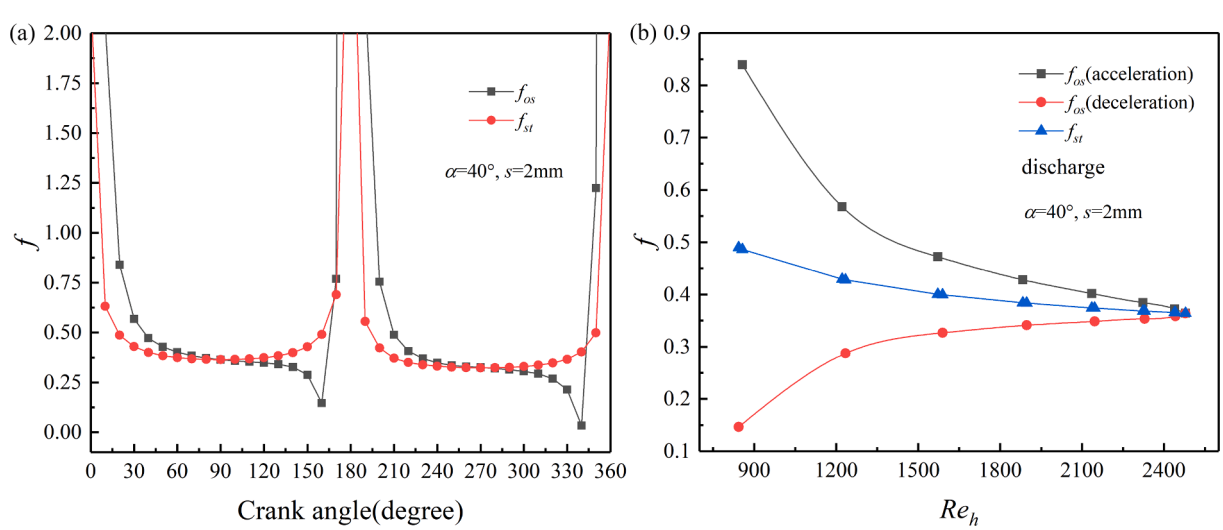

Fig. 18. Comparison of the oscillating flow friction factor and steady flow friction factor: (a) friction factor versus crank angles of a cycle and (b) friction factor versus Re_h in the discharge phase.

The dimensionless geometrical parameters are introduced to obtain two master correlation equations of friction factor (one for discharge phase and one for suction phase) and two master correlation equations of Nusselt number (one for discharge phase and one for suction phase). The dimensionless pitch S and dimensionless inclined angle A are defined as follows:

$$S = s/d_w \tag{27}$$

$$A = sin\alpha \tag{28}$$

The four master correlation equations are shown as:

Friction factor: (Eq. (29) for discharge phase and Eq. (30) for suction phase)

$$f_{st} = (0.195 + 0.447A^{2.829})(70.83 + 73.9S^{2.482})/Re_h + (4.87 - 5.19A^{0.0946})(4.15 - 5.226S^{0.459}) \tag{29}$$

$$f_{st} = (0.054 + 0.679A^{3.064})(69.8 + 74.2S^{2.451})/Re_h + (3.72 - 6.85A^{0.794})(5.24 - 5.294S^{0.056}) \tag{30}$$

Nusselt number: (Eq. (31) for discharge phase and Eq. (32) for suction phase)

$$Nu = (0.0014 + 0.0052A)(1.734 + 0.481S)Re_h^{0.93} + (0.026 + 0.0757A^{0.995})(18.64 + 18.63S^{0.95}) \tag{31}$$

$$Nu = (0.0001 + 0.0012A)(1.698 + 1.697S)Re_h^{0.9984} + (0.143 + 0.1427A^{1.0037})(8.42 + 8.497S^{1.0017}) \tag{32}$$

The master correlation equations are supposed to predict the flow and heat transfer performance of the constructal bifurcation regenerators with various geometrical structures. Fig. 25 presents the comparisons of the results of simulation and the correlation equation predictions. The maximum deviations of friction factor are 5% and 6.4% for discharge phase and suction phase, respectively. For the Nusselt number, the deviations of the discharge and suction phases are less than 11.9% and 16.5%, respectively.

To demonstrate the accuracy of the conversion of the correlation equations into porous parameters, an equivalent porous model of the constructal bifurcation regenerator is built using the porous parameters obtained from the correlation equations. And a simulation is conducted to investigate the thermo-hydraulic performance of the porous model under the same conditions and numerical methods. The variations of the friction factor and Nusselt number in a cycle are compared between the porous media regenerator model and the regenerator with the actual geometry, as illustrated in Fig. 26. It can be observed that the friction factor obtained from the porous media regenerator model shows a good correspondence with that of the regenerator with the actual geometry. For the Nusselt number, as the velocity on the boundary approaches 0, the fluid flow driven by the inertial effect in the regenerator is not accurately predicted by the porous model, thus, the Nusselt number of the porous model is lower than that of the regenerator with the actual geometry. However, at most moments of the cycle, the heat transfer performance of them is in good agreement. Therefore, the conversion of the correlation equations into porous parameters in this paper can be regarded to be successful.

4.4. Comparison with the existing regenerators

The comparisons of friction factor and Nusselt number between the constructal bifurcation regenerator and the existing regenerators,

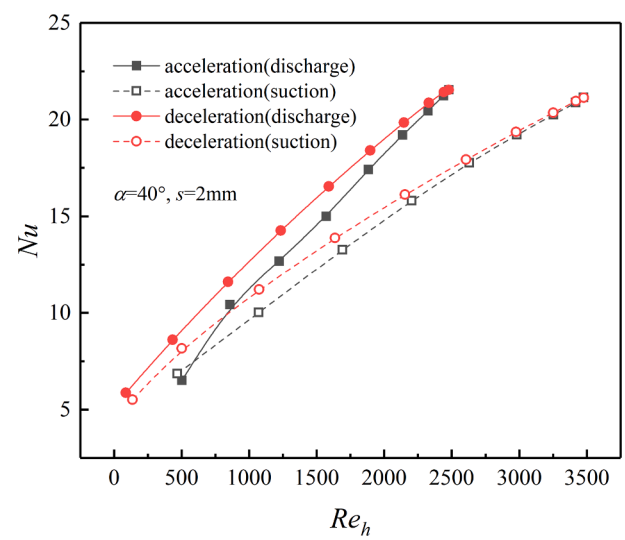

Fig. 20. Nusselt number in four different phases of a cycle.

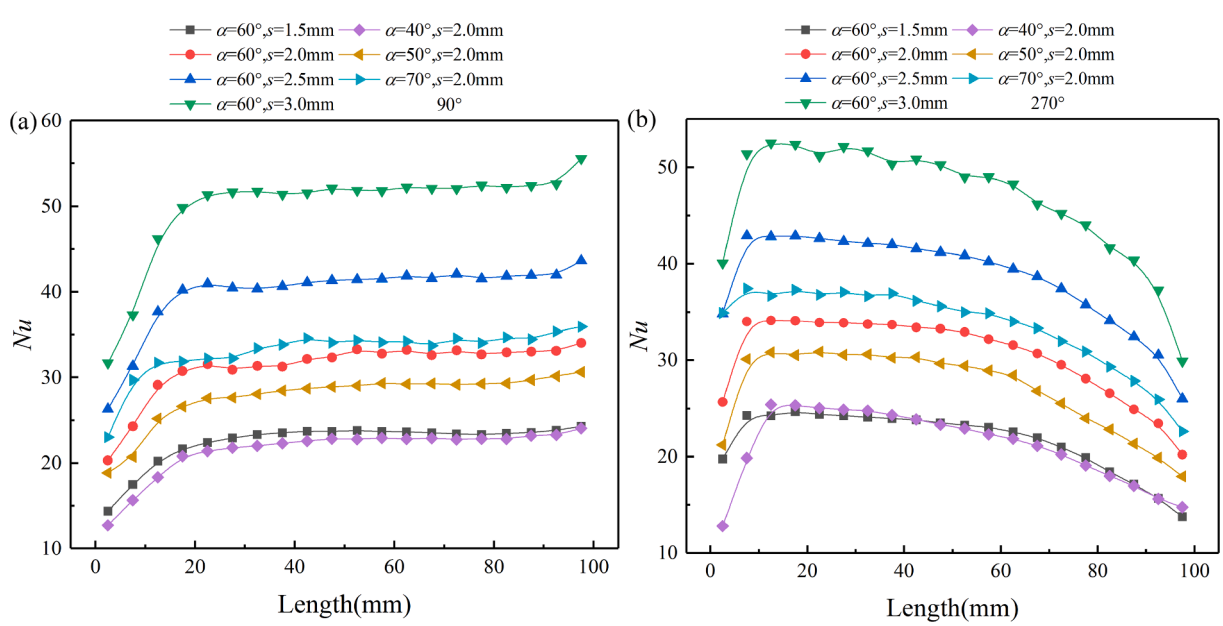

Fig. 19. Distributions of the local Nusselt number along the flow direction in the regenerator: (a) $\theta = 90°$ and (b) $\theta = 270°$.

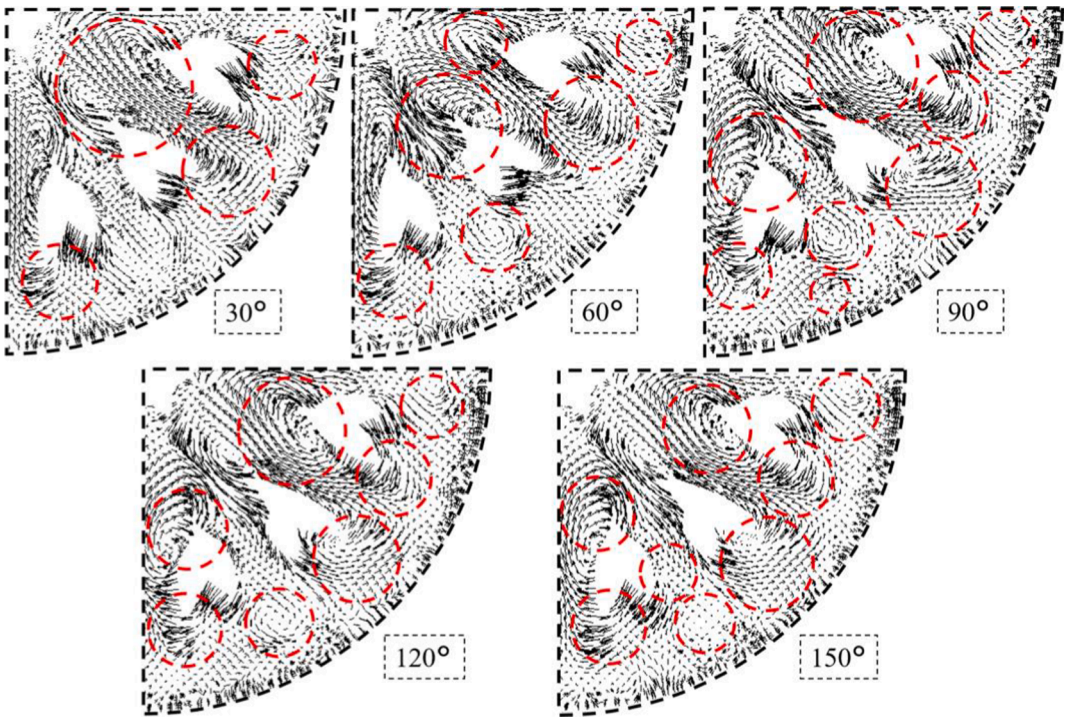

Fig. 21. Velocity vector at the middle cross-section under different crank angles ($\alpha = 40°$, $s = 2$ mm).

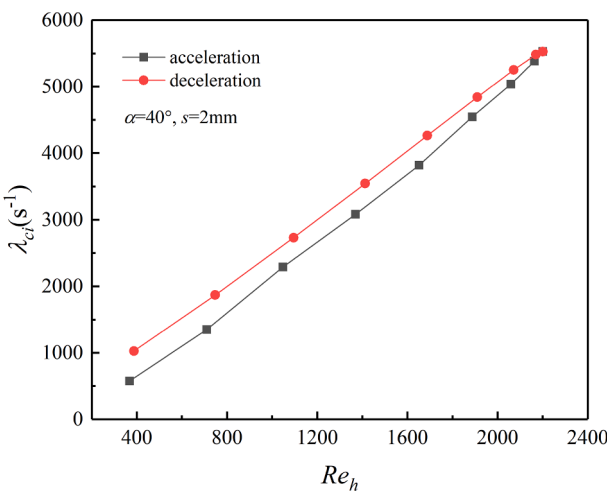

Fig. 22. Swirling strength λ_{ci} at the middle cross-section in the discharge phase.

including the regenerators made of stacked woven screens (Gedeon et al. [11], Tanaka et al. [12]), metal felts (Gedeon et al. [11]), arrays of pillars (Dellali et al. [32]), miniature-channels (Alfarawi et al. [6]), wound woven screens (Costa et al. [19]), and involute foils (Ibrahim et al. [29]), are presented in Fig. 27. The correlation equations of friction factor and Nusselt number for these regenerators are summarized in Table 5. According to Fig. 27, it is observed that the flow resistance of the constructal bifurcation regenerator is slightly higher than that of the involute foils regenerator and miniature-channels regenerator, but significantly lower than that of the conventional regenerators such as the woven screen regenerators and the metal felt regenerators. With respect to heat transfer performance, the constructal bifurcation regenerator has a larger structure scale and lower ability to disturb fluid than the conventional regenerators, which leads to the lower heat transfer performance. However, compared with the parallel miniature-channels regenerator, the constructal bifurcation regenerator gets a higher Nusselt number. Therefore, it can be concluded that the constructal bifurcation regenerator has relatively low flow resistance and moderate heat transfer performance, and thus achieves a relatively high comprehensive performance.

5. Conclusion

A novel constructal bifurcation regenerator was developed based on constructal concept in this work. The pressure drop and heat transfer characteristics of oscillating flows through the constructal bifurcation regenerator with various geometrical parameters were numerically investigated. Some main conclusions are drawn as below:

1. The flow resistance and thermal performance of the constructal bifurcation regenerator in the acceleration and deceleration phases are significantly different. The local acceleration effect and the formation of eddies in the acceleration phase are the main causes of these differences. Additionally, the local acceleration effect has also been proven to be the main cause of the difference in pressure drop characteristics between the oscillating and steady flows.
2. In the discharge and suction phases, the regenerator matrix generates different windward surfaces to the fluid as the fluid flows in the opposite directions, which will lead to different interactions between the matrix and the fluid. In this study, compared with the suction phase, an 8–26% higher flow resistance and a 4–40% higher heat transfer performance are obtained in the discharge phase.
3. The geometrical parameters such as the wire mesh pitch and the inclined angle have a strong effect on the regenerator performance. As the wire mesh pitch and inclined angle raise, the flow resistance and heat transfer of the regenerator increase substantially. This should be resulted from the different flow patterns in the regenerator generated by the different geometrical structures.
4. The three-parameters correlation equations for the steady flow friction factor and Nusselt number under various geometrical parameters and flow phases, and four master correlation equations with geometrical parameter dependence were obtained for predicting the performance of regenerators with different geometrical structures.

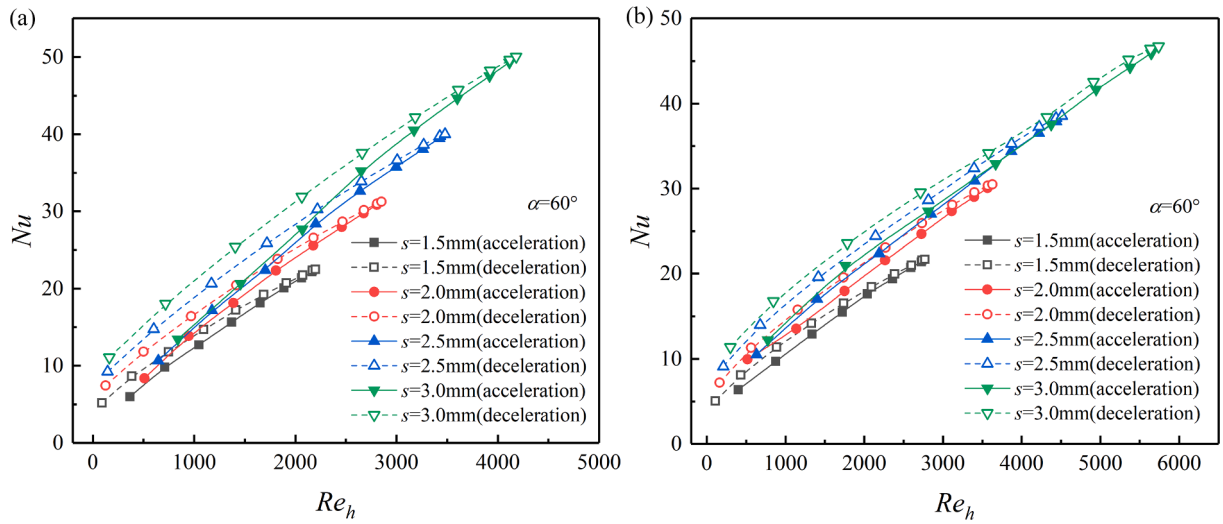

Fig. 23. Nusselt number under various wire mesh pitches: (a) discharge phase and (b) suction phase.

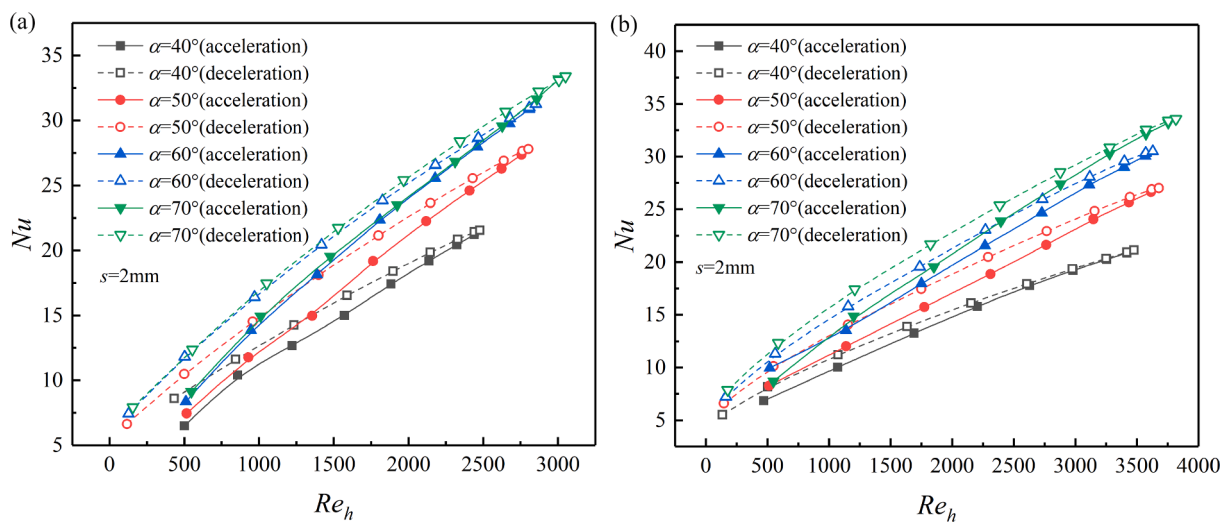

Fig. 24. Nusselt number under various inclined angles: (a) discharge phase and (b) suction phase.

Table 4
Correlation equations and porous parameters of the constructal bifurcation regenerators (Re_h = 500–6000).

Number/Phase		f_{st} correlation equations	Nu correlation equations	K	C_2
#1	discharge	$f_{st} = 113/Re_h + 0.3585Re_h^{0.05839}$	$Nu = 3.5992 + 0.02166Re_h^{0.8807}$	1.464×10^{-7}	$124.7Re_h^{0.05839}$
	suction	$f_{st} = 126.8/Re_h + 0.3377Re_h^{0.03263}$	$Nu = 3.5481 + 0.02636Re_h^{0.8251}$	1.305×10^{-7}	$117.4Re_h^{0.03263}$
#2	discharge	$f_{st} = 244.6/Re_h + 0.8191Re_h^{-0.01049}$	$Nu = 5.0015 + 0.02422Re_h^{0.8793}$	1.342×10^{-7}	$202.2Re_h^{-0.01049}$
	suction	$f_{st} = 231.4/Re_h + 0.8399Re_h^{-0.03}$	$Nu = 5.5677 + 0.02129Re_h^{0.8627}$	1.418×10^{-7}	$207.3Re_h^{-0.03}$
#3	discharge	$f_{st} = 408.1/Re_h + 0.8903Re_h^{0.00655}$	$Nu = 6.5664 + 0.01848Re_h^{0.9211}$	1.311×10^{-7}	$172.1Re_h^{0.00655}$
	suction	$f_{st} = 369.6/Re_h + 0.938Re_h^{-0.01694}$	$Nu = 6.5956 + 0.0203Re_h^{0.8753}$	1.448×10^{-7}	$181.3Re_h^{-0.01694}$
#4	discharge	$f_{st} = 598.2/Re_h + 0.8947Re_h^{0.02417}$	$Nu = 8.2331 + 0.01437Re_h^{0.9578}$	1.397×10^{-7}	$138.4Re_h^{0.02417}$
	suction	$f_{st} = 502.9/Re_h + 1.2861Re_h^{-0.03581}$	$Nu = 8.1501 + 0.0183Re_h^{0.8843}$	1.661×10^{-7}	$200Re_h^{-0.03581}$
#5	discharge	$f_{st} = 186.9/Re_h + 0.1706Re_h^{0.06762}$	$Nu = 3.0275 + 0.03102Re_h^{0.818}$	1.345×10^{-7}	$48.1Re_h^{0.06762}$
	suction	$f_{st} = 84.6/Re_h + 0.6115Re_h^{-0.08808}$	$Nu = 4.0308 + 0.02556Re_h^{0.7984}$	2.971×10^{-7}	$172.5Re_h^{-0.08808}$
#6	discharge	$f_{st} = 207.9/Re_h + 0.4317Re_h^{0.02889}$	$Nu = 5.0361 + 0.01101Re_h^{0.9628}$	1.501×10^{-7}	$109.3Re_h^{0.02889}$
	suction	$f_{st} = 177.6/Re_h + 0.3186Re_h^{0.05159}$	$Nu = 5.2749 + 0.01515Re_h^{0.8859}$	1.757×10^{-7}	$80.7Re_h^{0.05159}$
#7	discharge	$f_{st} = 313.8/Re_h + 0.8784Re_h^{-0.01147}$	$Nu = 5.1525 + 0.02462Re_h^{0.8787}$	1.237×10^{-7}	$199.4Re_h^{-0.01147}$
	suction	$f_{st} = 242.2/Re_h + 1.1313Re_h^{-0.04975}$	$Nu = 5.0998 + 0.02933Re_h^{0.835}$	1.602×10^{-7}	$256.8Re_h^{-0.04975}$

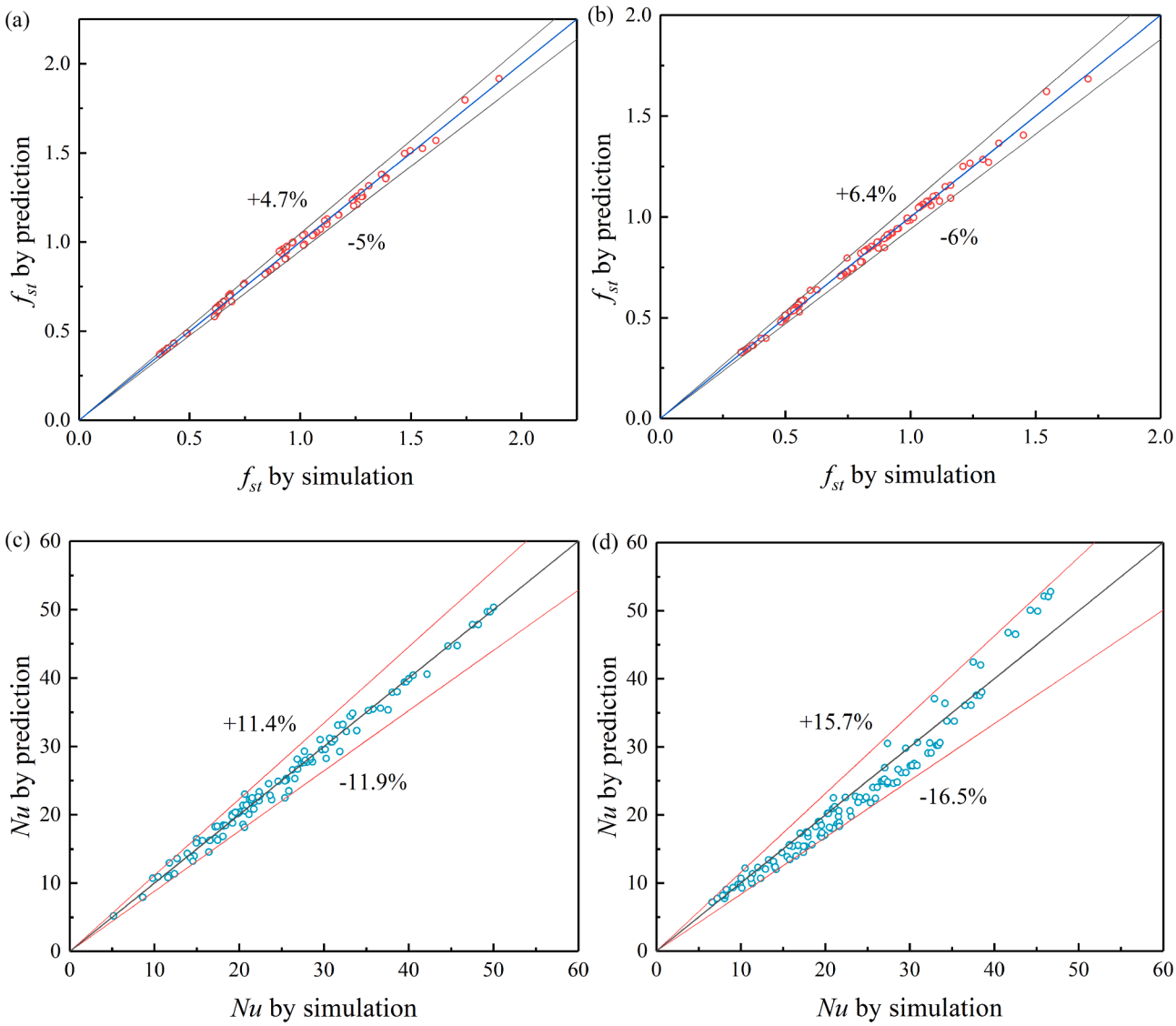

Fig. 25. Comparisons of the simulation results and the correlation equation predictions: (a) friction factor for discharge phase, (b) friction factor for suction phase, (c) Nusselt number for discharge phase and (d) Nusselt number for suction phase.

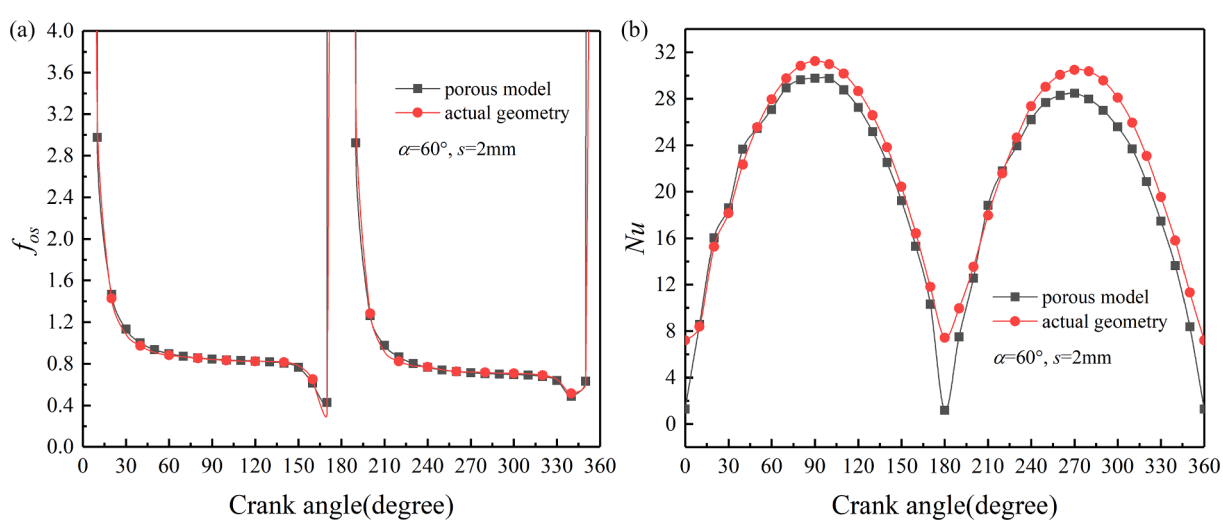

Fig. 26. Comparison of the thermo-hydraulic performance between the porous media regenerator model and the regenerator with the actual geometry: (a) oscillating flow friction factor and (b) Nusselt number.

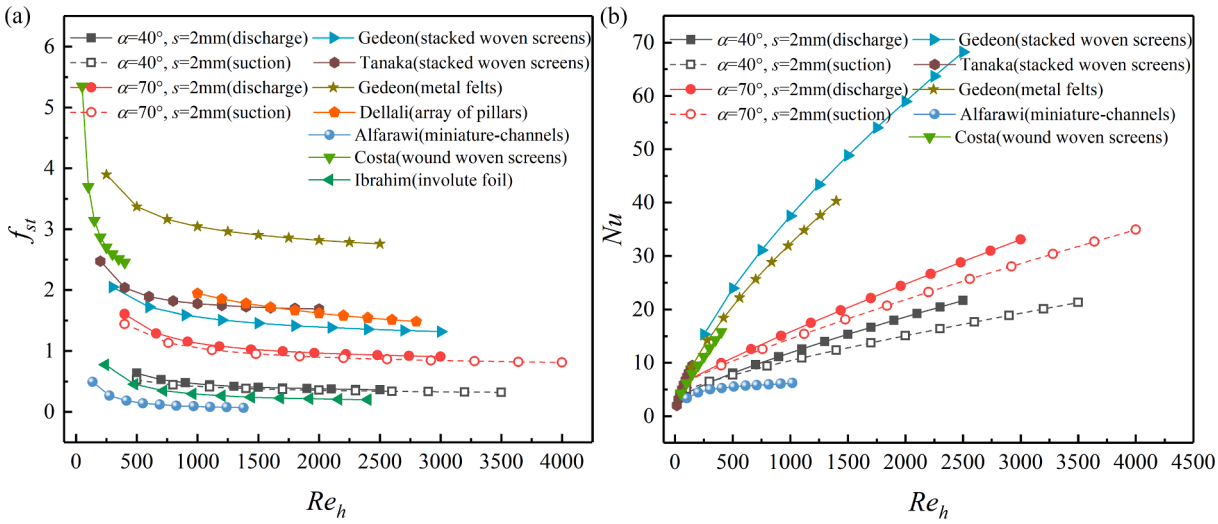

Fig. 27. Comparisons of flow and heat transfer between the constructal bifurcation regenerator and the existing regenerators: (a) friction factor and (b) Nusselt number.

Table 5
Correlations of friction factor and Nusselt number for the existing regenerators.

Authors	Regenerator type	Correlations	Conditions
Gedeon et al.	stacked woven screens	$f = 129/Re_h + 2.91Re_h^{-0.103}$ $Nu = [1 + 0.99(Re_hPr)^{0.66}]\gamma^{1.79}$	$Re_h = 0.45$–6100 $\gamma = 0.623$–0.78 $d_w = 53$–94 μm
Tanaka et al.	stacked woven screens	$f = 175/Re_h + 1.6$ $Nu = 0.33Re_h^{0.67}$	$Re_h = 10$–2000 $\gamma = 0.645$–0.754 $d_w = 50$–230 μm
Gedeon et al.	metal felts	$f = 192/Re_h + 4.53Re_h^{-0.067}$ $Nu = [1 + 1.16(Re_hPr)^{0.66}]\gamma^{2.61}$	$Re_h = 0.11$–2500 $\gamma = 0.688$–0.8405 $d_w = 12.7$–50.8 μm
Dellali et al.	arrays of pillars	$f = 11.88Re_h^{-0.262}$	$Re_h = 900$–6300 $\gamma = 0.8$–0.9 $d_h = 2.1$–3.7 mm
Alfarawi et al.	miniature-channels	$Nu = 1.143Re_h^{0.2488}$	$Re_h = 100$–1400 $\gamma = 0.391$ $d_h = 1$ mm
Costa et al.	wound woven screens	$f = 165.5/Re_h + 2.04$ $Nu = 2.15 + 0.07Re_h^{0.88}$	$Re_h = 4$–400 $\gamma = 0.6$–0.68 $d_w = 80$–110 μm
Ibrahim et al.	involute foils	$f = 153.1/Re_h + 0.127Re_h^{0.01}$	$Re_h = 207$–2400 $d_h = 4.87$ mm

The correlations were converted into equivalent porous parameters and the conversion has been proven to be successful.

5. Compared with other usually used regenerators, the constructal bifurcation regenerator has a low flow resistance and moderate heat transfer performance, and thus achieves a relatively high comprehensive performance, which makes it possible to improve the performance of Stirling engines. A further 3D CFD study on the Stirling engine embedded with the equivalent porous media model of the constructal bifurcation regenerator will follow this study to further validate the potential of the constructal bifurcation regenerator.

CRediT authorship contribution statement

Minjie Yu: Conceptualization, Methodology, Software, Validation, Formal analysis, Investigation, Data curation, Writing - original draft, Writing - review & editing, Visualization. **Feng Xin:** Methodology, Software, Data curation. **Xiaotian Lai:** Methodology, Software. **Hui Xiao:** Methodology, Software. **Zhichun Liu:** Resources, Supervision, Project administration, Funding acquisition. **Wei Liu:** Conceptualization, Resources, Supervision, Project administration, Funding acquisition.

Declaration of Competing Interest

The authors declare that they have no known competing financial interests or personal relationships that could have appeared to influence the work reported in this paper.

Acknowledgements

This work was supported by the National Natural Science Foundation of China (Grant No. 51736004).

References

[1] E. Santoyo, R. Best, M. López de Haro, The third international symposium on renewable energy and sustainability (ISRES 2015), Appl. Therm. Eng. 114 (2017) 1115–1118.
[2] M.A. Butturi, F. Lolli, M.A. Sellitto, E. Balugani, R. Gamberini, B. Rimini, Renewable energy in eco-industrial parks and urban-industrial symbiosis: A literature review and a conceptual synthesis, Appl. Energy 255 (2019) 113825.
[3] C. Çınar, F. Aksoy, H. Solmaz, E. Yılmaz, A. Uyumaz, Manufacturing and testing of an α-type Stirling engine, Appl. Therm. Eng. 130 (2018) 1373–1379.
[4] G. Xiao, U. Sultan, M. Ni, H. Peng, X. Zhou, S. Wang, Z. Luo, Design optimization with computational fluid dynamic analysis of β-type Stirling engine, Appl. Therm. Eng. 113 (2017) 87–102.
[5] K. Bataineh, Mathematical formulation of alpha -type Stirling engine with Ross Yoke mechanism, Energy 164 (2018) 1178–1199.
[6] S. Alfarawi, R. Al-Dadah, S. Mahmoud, Potentiality of new miniature-channels Stirling regenerator, Energy Convers. Manage. 133 (2017) 264–274.
[7] D.G. Thombare, S.K. Verma, Technological development in the Stirling cycle engines, Renew. Sustain. Energy Rev. 12 (2008) 1–38.
[8] S.K. Andersen, H. Carlsen, P.G. Thomsen, Preliminary results from simulations of temperature oscillations in Stirling engine regenerator matrices, Energy 31 (2006) 1371–1383.
[9] S.K. Andersen, H. Carlsen, P.G. Thomsen, Numerical study on optimal Stirling engine regenerator matrix designs taking into account the effects of matrix temperature oscillations, Energy Convers. Manage. 47 (2006) 894–908.
[10] D.D. Dai, F. Yuan, R. Long, Z.C. Liu, W. Liu, Imperfect regeneration analysis of Stirling engine caused by temperature differences in regenerator, Energy Convers. Manage. 158 (2018) 60–69.
[11] D. Gedeon, J.G. Wood, Oscillating-flow regenerator test rig: hardware and theory with derived correlations for screens and felts, NASA CR-198442 (1996) 6–13.
[12] M. Tanaka, I. Yamashita, F. Chisaka, Flow and heat transfer characteristics of the stirling engine regenerator in an oscillating Flow, JSME Int. J. 33 (1990) 283–289.
[13] R. Gheith, F. Aloui, S. Ben Nasrallah, Study of temperature distribution in a Stirling engine regenerator, Energy Convers. Manage. 88 (2014) 962–972.

[14] R. Gheith, F. Aloui, S. Ben Nasrallah, Determination of adequate regenerator for a Gamma-type Stirling engine, Appl. Energy 139 (2015) 272–280.
[15] W.-L. Chen, K.-L. Wong, H.-E. Chen, An experimental study on the performance of the moving regenerator for a γ-type twin power piston Stirling engine, Energy Convers. Manage. 77 (2014) 118–128.
[16] A.S. Nielsen, B.T. York, B.D. MacDonald, Stirling engine regenerators: How to attain over 95% regenerator effectiveness with sub-regenerators and thermal mass ratios, Appl. Energy 253 (2019) 113557.
[17] S.C. Costa, H. Barrutia, J.A. Esnaola, M. Tutar, Numerical study of the pressure drop phenomena in wound woven wire matrix of a Stirling regenerator, Energy Convers. Manage. 67 (2013) 57–65.
[18] S.C. Costa, H. Barrutia, J.A. Esnaola, M. Tutar, Numerical study of the heat transfer in wound woven wire matrix of a Stirling regenerator, Energy Convers. Manage. 79 (2014) 255–264.
[19] S.C. Costa, I. Barreno, M. Tutar, J.A. Esnaola, H. Barrutia, The thermal non-equilibrium porous media modelling for CFD study of woven wire matrix of a Stirling regenerator, Energy Convers. Manage. 89 (2015) 473–483.
[20] Z. Buliński, A. Kabaj, T. Krysiński, I. Szczygieł, W. Stanek, B. Rutczyk, L. Czarnowska, P. Gładysz, A Computational Fluid Dynamics analysis of the influence of the regenerator on the performance of the cold Stirling engine at different working conditions, Energy Convers. Manage. 195 (2019) 125–138.
[21] W.-L. Chen, K.-L. Wong, Y.-F. Chang, A numerical study on the effects of moving regenerator to the performance of a β -type Stirling engine, Int. J. Heat Mass Transf. 83 (2015) 499–508.
[22] G. Xiao, H. Peng, H. Fan, U. Sultan, M. Ni, Characteristics of steady and oscillating flows through regenerator, Int. J. Heat Mass Transf. 108 (2017) 309–321.
[23] S.-C. Costa, M. Tutar, I. Barreno, J.-A. Esnaola, H. Barrutia, D. García, M.-A. González, J.-I. Prieto, Experimental and numerical flow investigation of Stirling engine regenerator, Energy 72 (2014) 800–812.
[24] R. Radebaugh, B. Louie, A simple, first step to the optimization of regenerator geometry, in: In its Proc of the 3rd Cryocooler Conf, 1985, pp. 177–198.
[25] K. Nam, S. Jeong, Development of parallel wire regenerator for cryocoolers, Cryogenics 46 (2006) 278–287.
[26] Z. Li, Y. Haramura, D. Tang, C. Guo, Analysis on the heat transfer characteristics of a micro-channel type porous-sheets Stirling regenerator, Int. J. Therm. Sci. 94 (2015) 37–49.
[27] S. Alfarawi, R. Al-Dadah, S. Mahmoud, Transient investigation of mini-channel regenerative heat exchangers: Combined experimental and CFD approach, Appl. Therm. Eng. 125 (2017) 346–358.
[28] K. Yanaga, R. Li, S. Qiu, Robust foil regenerator flow loss and heat transfer tests under oscillating flow condition, Appl. Therm. Eng. 178 (2020) 115525.
[29] M.B. Ibrahim, D. Danila, T. Simon, S. Mantell, L.Y. Sun, A Microfabricated Segmented-Involute-Foil Regenerator for Enhancing Reliability and Performance of Stirling Engines: Phase II Final Report for the Radioisotope Power Conversion Technology NRA Contract NAS3-03124, (2007) 53–59.
[30] S. Isshiki, H. Sato, S. Konno, H. Shiraishi, N. Isshiki, L. Fujii, H. Mizui, The Experimental Study of atmospheric Stirling engines using pin-fin arrays' heat exchangers, J. Power Energy Syst. 2 (2008) 1198–1208.
[31] A.M. Mancisidor, E. Gil, F. Garciandia, M.S. Sebastian, O. Lizaso, M. Escubi, Stirling engine regenerator based on lattice structures manufactured by selective laser melting, Procedia CIRP 74 (2018) 72–75.
[32] E. Dellali, S. Bégot, F. Lanzetta, E. Gavignet, J.Y. Rauch, Pressure drop analysis of oscillating flows through a miniature porous regenerator under isothermal and nonisothermal conditions, Exp. Therm Fluid Sci. 103 (2019) 394–405.
[33] L. Chen, Progress in study on constructal theory and its applications, Sci. China Technol. Sci. 55 (2012) 802–820.
[34] H. Feng, L. Chen, Z. Xie, Multi-disciplinary, multi-objective and multi-scale constructal optimizations for heat and mass transfer processes performed in Naval University of Engineering, a review, Int. J. Heat Mass Transf. 115 (2017) 86–98.
[35] H. Feng, C. Cai, L. Chen, Z. Wu, G. Lorenzini, Constructal design of a shell-and-tube condenser with ammonia-water working fluid, Int. Commun. Heat Mass Transfer 118 (2020) 104867.
[36] Z. Lu, K. Zhang, J. Liu, F. Li, Effect of branching level on the performance of constructal theory based Y-shaped liquid cooling heat sink, Appl. Therm. Eng. 168 (2020) 114824.
[37] H. Feng, Z. Xie, L. Chen, Z. Wu, S. Xia, Constructal design for supercharged boiler superheater, Energy 191 (2020) 116484.
[38] L. Chen, Q. Xiao, Z. Xie, F. Sun, Constructal entransy dissipation rate minimization for tree-shaped assembly of fins, Int. J. Heat Mass Transf. 67 (2013) 506–513.
[39] J. Yang, A. Fan, W. Liu, A.M. Jacobi, Optimization of shell-and-tube heat exchangers conforming to TEMA standards with designs motivated by constructal theory, Energy Convers. Manage. 78 (2014) 468–476.
[40] L. Chen, H. Feng, Z. Xie, F. Sun, Progress of constructal theory in China over the past decade, Int. J. Heat Mass Transf. 130 (2019) 393–419.
[41] F. Xin, Z. Liu, N. Zheng, P. Liu, W. Liu, Numerical study on flow characteristics and heat transfer enhancement of oscillatory flow in a spirally corrugated tube, Int. J. Heat Mass Transf. 127 (2018) 402–413.
[42] C. Chi, J. Mou, M. Lin, G. Hong, CFD simulation and investigation on the operating mechanism of a beta-type free piston Stirling engine, Appl. Therm. Eng. 166 (2020) 114751.
[43] F. Xin, Z. Liu, S. Wang, W. Liu, Study of heat transfer in oscillatory flow for a Stirling engine heating tube inserted with spiral spring, Appl. Therm. Eng. 143 (2018) 182–192.
[44] M. Tutar, A. Holdø, Computational modelling of flow around a circular cylinder in sub-critical flow regime with various turbulence models, Int. J. Numer. Meth. Fluids 35 (2001) 763–784.
[45] X. Wang, M. Zhao, J. Cai, J. Liang, W. Dai, Experimental flow characteristics study of a high frequency pulse tube regenerator, in: Cryocoolers 13, Springer, 2005, pp. 439–444.
[46] S. Isshiki, Y. Takasaki, I. Ushiyama, An experimental study on flow resistance of regenerator wire meshes in oscillatory flow, in: Energy Conversion Engineering Conference, 1997. IECEC-97, Proceedings of the 32nd Intersociety, 1997, pp. 1027–1032.
[47] J. Zhou, R.J. Adrian, S. Balachandar, T.M. Kendall, Mechanisms for generating coherent packets of hairpin vortices in channel flow, J. Fluid Mech. 387 (1999) 353–396.
[48] H. Chen, D. Li, R. Bai, X. Wang, Comparison of swirling strengths derived from two- and three-dimensional velocity fields in channel flow, AIP Adv. 8 (2018) 055302.